

RESEARCH ARTICLE

CDK actively contributes to establishment of the stationary phase state in fission yeast

Motoaki Hiraoka, Yuki Kiyota, Shinnosuke Kawai, Yusuke Notsu, Kohei Yamada, Katsuyuki Kurashima, Jing-Wen Chang, Shunsuke Shimazaki and Ayumu Yamamoto*

ABSTRACT

Upon exhaustion of essential environmental nutrients, unicellular organisms cease cell division and enter stationary phase, a metabolically repressed state essential for cell survival in stressful environments. In the fission yeast *Schizosaccharomyces pombe*, cell size is reduced by cell division before entry into stationary phase; thus cyclin-dependent kinase (CDK) must actively contribute to stationary phase establishment. However, the contribution of CDK to stationary phase remains largely uncharacterized. Here, we examine the role of the sole *S. pombe* CDK, Cdc2, in the establishment of stationary phase. We show that in stationary phase, nuclear and chromosomal volumes and the nucleus-to-cell volume ratio are reduced, and sister chromatid separation and chromosome fluctuation are repressed. Furthermore, Cdc2 accumulates in the nucleolus. Most of these changes are induced by glucose depletion. Reduction in Cdc2 activity before and upon stationary phase entry alleviates the changes and shortens the survival time of stationary phase cells, whereas Cdc2 inhibition represses nucleolar Cdc2 accumulation and glucose depletion-induced nuclear volume reduction. These results demonstrate that CDK actively regulates stationary phase, both before and upon stationary phase entry.

KEY WORDS: Quiescence, Fission yeast, Stationary phase, Cyclin-dependent kinase, Glucose, Nucleus

INTRODUCTION

Quiescence is the non-dividing but proliferation-competent state observed in all living organisms (Broach, 2012; De Virgilio, 2012; Gray et al., 2004; Herman, 2002; Marescal and Cheeseman, 2020; O'Farrell, 2011; Rittershaus et al., 2013; Roche et al., 2017; Sagot and Laporte, 2019; Sun and Buttitta, 2017; Sun and Gresham, 2021; Valcourt et al., 2012; van Velthoven and Rando, 2019; Velappan et al., 2017; Yanagida, 2009). Cells enter quiescence in response to various extracellular stimuli, including growth inhibitory signals and nutrient starvation, and quiescent cells restart cell division upon receiving appropriate stimuli or restoration of growth-suitable environments. In multicellular organisms, various non-differentiated stem cells and many differentiated cells including dermal fibroblasts, lymphocytes, and hepatocytes are in the

quiescent state. A large majority of microorganisms in nature are in the quiescent state (Cole, 1999; Rittershaus et al., 2013). Cells of unicellular organisms enter the quiescent state, termed the 'stationary phase', upon nutrient exhaustion (Gray et al., 2004; Yanagida, 2009; Broach, 2012; Sagot and Laporte, 2019; Sun and Gresham, 2021). Quiescent cells are characterized by the substantial repression of their metabolic activity and their resistance to various stresses, and such characteristics are crucial for organisms to survive in stressful and/or nutrient-limited environments. In addition, the drug resistance of quiescent cancer cells or pathogens represents a major obstacle for treatment of several tumors and infectious diseases (Bojsen et al., 2017; Borst, 2012; Rittershaus et al., 2013). Therefore, understanding the molecular basis of quiescence is both biologically and clinically important.


Studies of stationary phase in yeast have demonstrated that the stationary phase state is markedly distinct from that of cycling cells (Gray et al., 2004; Klosinska et al., 2011; Rittershaus et al., 2013; Werner-Washburne et al., 1993). In stationary phase cells, numerous distinct types of granules, which contain mRNAs, signaling molecules, metabolic enzymes and/or proteasomes, form in the cytoplasm, (Bregues et al., 2005; Laporte et al., 2008, 2011; Narayanaswamy et al., 2009; Nostramo et al., 2016; Shah et al., 2014). Dynamic cytoskeletal filaments turn into immobile, non-dynamic filaments or aggregates (Laporte et al., 2013, 2015; Sagot et al., 2006), whereas chromosomes become condensed with a decrease in their Brownian-like fluctuation (hereafter called chromosome fluctuation) and change their intranuclear positioning, and the cytoplasm becomes solidified (Heimlicher et al., 2019; Joyner et al., 2016; Laporte et al., 2016; Piñon, 1978; Rutledge et al., 2015).

Stationary phase establishment is coupled with the cell cycle. Yeast cells become smaller in size by the modulation of the preceding cell cycle (Gray et al., 2004; Yanagida et al., 2011). In addition, although glucose starvation induces entry into stationary phase, acute glucose depletion, which immediately terminates the cell cycle, fails to induce some stationary phase-associated changes. For instance, after acute glucose depletion, budding yeast cells do not show resistance to cell wall-digesting enzymes, a common stationary phase characteristic, whereas in fission yeast, cell size reduction does not occur (Klosinska et al., 2011; Yanagida, 2009). Given that the decreased concentration of glucose in the growth medium induces some stationary phase-associated phenotypes in cycling cells (Kelkar and Martin, 2015; Klosinska et al., 2011; Pluskal et al., 2011), the gradual decline in environmental nutrients during cell proliferation probably induces modulation of the preceding cell cycle, which thus contributes to the stationary phase establishment.

Given the central role of cyclin-dependent kinase (CDK) in the cell cycle, CDK must actively contribute to cell cycle modulation in order to establish the stationary phase state. Indeed, in *Schizosaccharomyces pombe*, several signaling kinases, such as

Graduate School of Integrated Science and Technology, Shizuoka University, 836 Ohya, Suruga-ku, Shizuoka 422-8529, Japan.

*Author for correspondence (yamamoto.ayumu@shizuoka.ac.jp)

 M.H., 0000-0002-8131-5367; Y.K., 0000-0001-7294-1350; Y.N., 0000-0002-1884-1735; K.Y., 0000-0002-1827-1621; A.Y., 0000-0001-6960-9461

Handling Editor: David Glover

Received 17 October 2022; Accepted 21 April 2023

TOR, PKA, and MAPKs, which are responsible for the establishment of stationary phase (De Virgilio, 2012; Gray et al., 2004; Herman, 2002; Yanagida, 2009), regulate the sole *S. pombe* CDK, Cdc2, to reduce cell size in response to nutrient limitation (Kelkar and Martin, 2015; Petersen and Nurse, 2007; Yanagida et al., 2011). In addition, CDK and its regulators are important for survival of stationary phase *S. pombe* cells under nutrient-starved conditions (Masuda et al., 2016). However, given that cell cycle arrest is a hallmark of quiescence, many previous studies on nutrient-induced quiescence in yeast have focused on the role of CDK inhibition in quiescence establishment (Moreno-Torres et al., 2015; Simanis and Nurse, 1986; Werner-Washburne et al., 1993; Yanagida, 2009; Zinzalla et al., 2007). Therefore, the active contribution of CDK to the stationary phase establishment remains largely unstudied. In this study, we examine the stationary phase state of *S. pombe* and the contribution of CDK to its establishment, and show that CDK actively contributes to the establishment of the stationary phase state.

RESULTS

Nuclear area and chromosome-occupying space are reduced in stationary phase

To understand how CDK functions in the establishment of stationary phase in *S. pombe*, we first characterized the stationary phase state by examining the morphology and size of the nucleus

and chromosomes, which dynamically change during the cell cycle under CDK control and become smaller or condensed in quiescent cells of various organisms (Evertts et al., 2013; Faire et al., 2015; Guidi et al., 2015; Gupta et al., 2012; Piñon, 1978; Rawlings et al., 2011; Rutledge et al., 2015; Sajiki et al., 2009; Schäfer et al., 2008; Su et al., 1996; Swygert et al., 2019). A GFP-tagged N-terminal portion of cytochrome *c* reductase (Fig. 1A) (Ding et al., 2000; Nambu et al., 2022) and an mCherry-tagged histone H2A were used to visualize the nuclear envelope and chromosomes, respectively, and nuclear and chromosomal size was analyzed by measuring the area of the nucleus and of the chromosome-occupying space in the two-dimensional images or by calculating nuclear volume from the nuclear image. In this study, cells were grown in YES-rich medium and not minimal medium, as cells enter the stationary phase exclusively from G2 in the YES-rich medium (Fig. S1A), but from both G1 and G2 in the minimal medium (Yanagida, 2009). In addition, for evaluation of both exponentially growing (log phase) and stationary phase cells, only cells containing a single nucleus with non-condensed chromosomes, which are in G2 (Hayles and Nurse, 2018), were analyzed, to exclude cell cycle-associated nuclear and chromosomal changes.

In log phase, the majority of cells contained a single nucleus with non-condensed chromosomes (78.0%, $n=118$). In these cells, the nucleus was located at the center of the cell, and the chromosomes

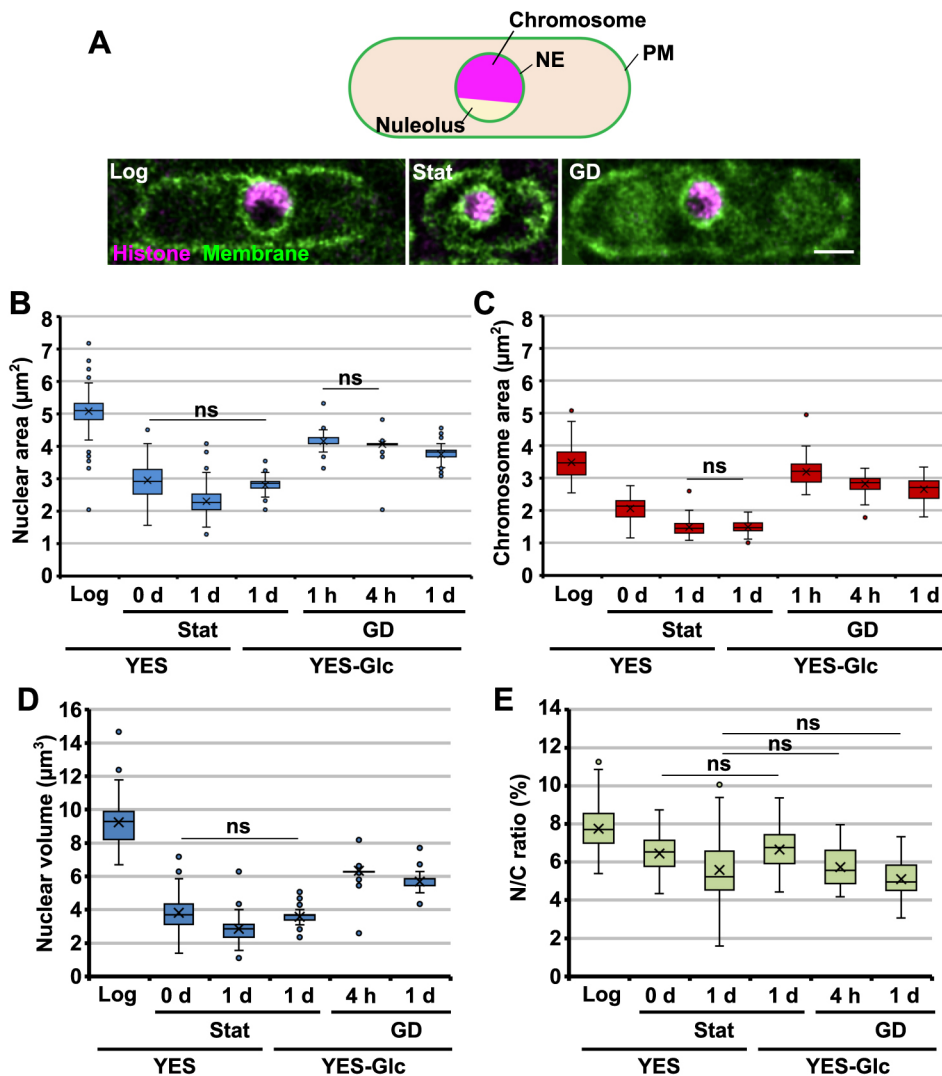


Fig. 1. Changes in nuclear size and chromosome-occupying space in stationary phase and GD cells. (A) The nucleus and chromosomes in cells.

Schematic diagram shows the plasma membrane (PM), the nuclear envelope (NE), and chromosomes (chromosome) in an *S. pombe* cell. In micrographs, green shows PM and NE visualized by Ccr1-N-GFP and magenta shows chromosomes visualized by mCherry-tagged histone H2A (Hta1-mCherry). Scale bar: 2 µm. (B,C) Area of the nucleus (B) and a chromosome-occupying space (C) in log phase (Log), stationary phase (Stat), and GD cells (GD). More than 80 cells were examined for each analysis. (D) Nuclear volume. (E) The N/C ratio. In D and E, more than 50 cells were examined for each analysis. Area and volume were measured at indicated time points after entry into stationary phase or transfer to YES-Glc medium. For all box and whiskers plots, the box indicates the interquartile range of the data set (IQR), whiskers show the rest of the distribution within 1.5× IQR, circles outside of whiskers show outliers, and the cross indicates the mean value. All statistical analyses were carried out using the unpaired, two-tailed Student's *t*-test with the Bonferroni correction (Fig. S1D–G). Lines show pairs with no significant difference (ns; $P>0.05$).

occupied a hemispherical intranuclear space (Fig. 1A), as reported previously (Toda et al., 1981). In stationary phase, cells were shorter and smaller in volume than in log phase (Fig. S1B,C,H,I), and most of them contained a single nucleus (91.3%, $n=103$), in which the chromosomes occupied a hemispherical space (Fig. 1A). However, area or volume analysis of the nucleus and the chromosome-occupying space showed that nuclear and chromosomal sizes were significantly smaller (Fig. 1B–D; Fig. S1D–F), as seen in quiescence induced by nitrogen starvation (Sajiki et al., 2009; Su et al., 1996). The nuclear and chromosomal sizes continued to decrease for at least 1 day after entry into stationary phase, and the nuclear size became less than one third of the original size. Furthermore, the nuclear to cell volume ratio (N/C ratio), which has been reported to be constant irrespective of cell size (Neumann and Nurse, 2007), was significantly smaller (Fig. 1E; Fig. S1G). Thus, the nuclear size reduction observed in stationary phase cells did not originate simply from the reduction in cell size.

In glucose-rich medium, glucose exhaustion is thought to induce entry into stationary phase. To explore the contribution of the preceding cell cycle to establishment of the stationary phase state, we next examined the cell state induced by acute glucose depletion, which causes immediate cell cycle arrest (hereafter, cells responding to acute glucose depletion and their state are called GD cells and GD state, respectively) (Yanagida, 2009). Log phase cells were transferred to YES medium lacking glucose (YES-Glc) and their nuclear and chromosomal sizes were examined. The immediate cell cycle arrest induced by glucose depletion did not cause cell size reduction (Fig. 1A; Fig. S1B,C,H,I). In these cells, the nuclear and chromosomal sizes became significantly smaller than in the log phase cells, but not as small as those in stationary phase cells (Fig. 1B–D; Fig. S1D–F). The N/C ratio was also reduced but not significantly different from that of stationary phase cells (Fig. 1E; Fig. S1G), suggesting that the observed nuclear size differences from stationary phase originate from the cell size differences. Furthermore, incubation of stationary phase cells in fresh YES-Glc medium immediately after entry into the stationary phase did not cause a further reduction in nuclear size or N/C ratio (Fig. 1B,D,E, Stat, 1 d, YES-Glc; Fig. S1D,F,G). This indicates that stationary phase cells can sustain nuclear size by utilizing nutrients.

The association of sister chromatids is changed in stationary phase

The fact that *S. pombe* cells enter stationary phase exclusively from G2 prompted us to investigate the effect of entry into stationary phase on the association of sister chromatids. We examined the association state of three chromosomal loci on distinct chromosomes visualized using a GFP-tagged *lac* repressor (Fig. 2A) (Ding et al., 2004; Nabeshima et al., 1998; Yamamoto and Hiraoka, 2003). The *nda3* β -tubulin gene promoter was used for expression of the *lac* repressor, thus enabling chromosome visualization in both stationary and log phase cells. We also avoided using the nuclear localization sequence (NLS) to direct the *lac* repressor to the nucleus, as the NLS was not essential for nuclear localization of the repressor and appeared to obscure changes in the association state of sister chromatids in stationary phase (see below), although the reasons for this are unclear. We simultaneously visualized microtubules to exclude spindle-forming log phase cells that were in the process of sister chromatid separation.

In contrast to the accepted view that sister chromatids are tightly associated with each other along their entire length before anaphase, all examined sister loci were separated in $\sim 10\%$ of cells in log phase (Fig. 2B,C, Log). This result indicates that sister chromatids occasionally undergo partial separation. After entry into stationary

phase, G2 cytoplasmic microtubules converted into one or more short, thick microtubule bundles, as reported previously (Laporte et al., 2015). In these cells, although sister locus separation occurred (Fig. 2B), the frequency with which these separations were observed significantly decreased at all assessed loci (Fig. 2C). This suggests that sister chromatids become more tightly associated with each other in the stationary phase. At 1 day after entry into stationary phase, the separation frequencies of the *nhe1* and *ade6* loci remained reduced, whereas that of the *ade8* locus returned to log phase levels, indicating that the tight association was transient at some loci. Although we cannot completely exclude the possibility that sister locus separation and its repression are artifacts generated by the *lac/lacO* chromosome visualization, these results suggest that the chromosomal association state is distinct in stationary phase. By contrast, separation frequencies did not decline in GD cells (Fig. 2B,C, GD), suggesting that acute glucose depletion does not alter the association state of sister chromatids.

Chromosome fluctuations are decreased in the stationary phase

In budding yeast, chromosome loci exhibit Brownian-like fluctuation in the nucleus, and this fluctuation is decreased upon glucose depletion (Joyner et al., 2016). We therefore wished to examine whether chromosome fluctuation is similarly repressed in stationary phase in *S. pombe* cells. Images of the GFP-visualized loci were captured in three dimensions every 1.5 s and changes in their positioning over time were analyzed. The visualized loci changed their position over time in log phase cells (Fig. 2D, Log), indicating that chromosomes fluctuate as in budding yeast. In addition, the sister loci often underwent transient separation, indicating that separation of the sister loci seen in still images reflects their transient separation. Separation behavior varied among observations; separation was rare in some observations but very frequent in others (Fig. 2D, Log), suggesting that association varies between cells or stages. By contrast, in stationary phase, the visualized sister chromatid loci appeared to be less mobile, and their separation was rare (Fig. 2D, Stat). Plots of the mean square displacement (MSD) of the loci demonstrated that fluctuation mobilities varied among the loci (Fig. 2E; Fig. S2A). However, the fluctuation mobilities of all examined loci were significantly reduced in stationary phase compared to log phase, as demonstrated by a downshift of the stationary phase plots and an almost complete lack of an overlap of their 95% confidence intervals with those of the log phase plots during the 30 s observation (Fig. 2E). These results indicate that chromosome fluctuation is repressed in the stationary phase. Furthermore, the MSD plots of the loci in GD cells and their 95% confidence intervals showed that chromosome fluctuation was significantly repressed to the same level as in stationary phase (Fig. 2E). Considering the spatial scales of the fluctuation, this fluctuation repression cannot be attributed simply to spatial confinement. This conclusion is supported by simple numerical simulations of a particle diffusing in confined spherical spaces, which reflect the observed nuclear sizes in log and stationary phases (Fig. S2B). These results indicate that glucose depletion causes repression of chromosome mobility.

CDK accumulates in the nucleolus in stationary phase cells

We next examined the intracellular localization of Cdc2, the sole CDK in *S. pombe*. Consistent with a previous report (Decottignies et al., 2001), during log phase, Cdc2, together with Cdc13 (the *S. pombe* B-type cyclin), was evenly distributed across the nucleus of a mono-nuclear cell and frequently accumulated at a point, which corresponds to the SPB (Fig. 3A–C, Log). However, upon entering stationary phase, Cdc2 accumulated at the periphery of the

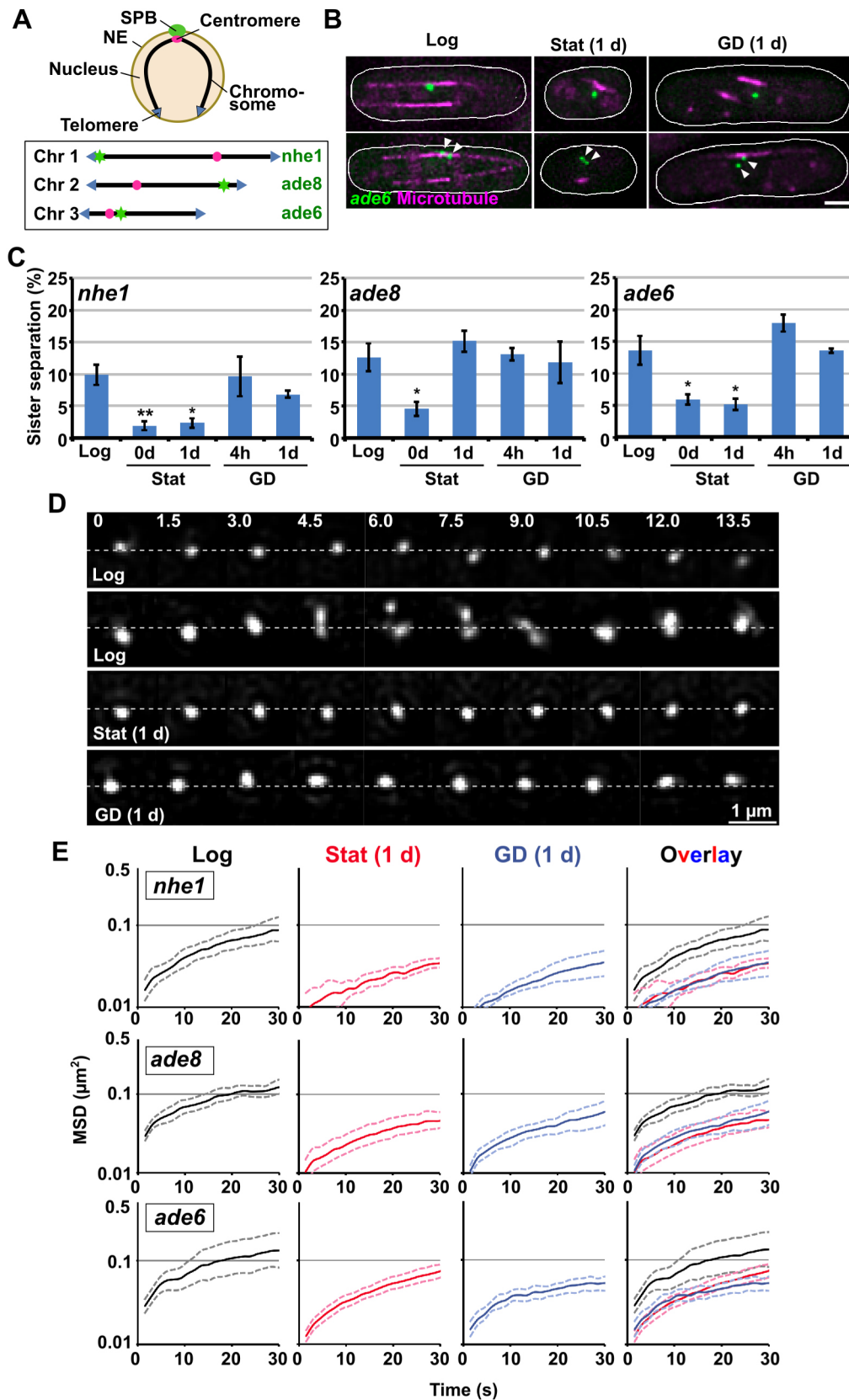


Fig. 2. Changes in sister chromatid association and chromosome fluctuation in stationary phase and after acute glucose depletion. (A) Analyzed chromosome loci.

Upper illustration shows intranuclear chromosome organization. Bottom illustration shows positions of labeled chromosome loci on three different chromosomes. The *nhe1* and the *ade8* loci are 0.05 and 0.35 Mb away from the telomeres, respectively, and the *ade6* locus is 0.18 Mb away from the centromere. (B) Associated (upper image) and separated (lower image) sister chromatid loci. The *ade6* locus and microtubules are shown in green and magenta, respectively. White lines indicate cell outlines. Arrowheads indicate separated sister loci. Scale bar: 2 μm . (C) Separation frequencies of sister loci. More than 70 cells were examined, and data represent mean \pm s.e.m. from at least three independent experiments. Asterisks indicate significant difference from log phase cells (* P <0.05; ** P <0.001 by unpaired, two-tailed Student's t -test). (D) Changes in positions of sister loci over time. Images of the GFP-visualized sister *ade8* loci were captured every 1.5 s. Numbers indicate time in seconds. Dotted lines indicate reference lines for sister locus positions. Scale bar: 1 μm . (E) The mean square displacement of the visualized chromosome loci. Dotted lines indicate 95% confidence intervals obtained by the bootstrap method. More than 11 cells were examined for each plot. Log, log phase cells; Stat, stationary phase cells at indicated time points after entry into stationary phase; GD, GD cells incubated in YES-Glc medium for indicated times.

chromosome-unoccupied, nucleolar region with a convex localization pattern (Fig. 3A–C, Stat). At 1 day after entry into stationary phase, Cdc2 became localized at two distinct regions in approximately half of cells analyzed (54.2%, $n=72$) (Fig. 3A, Stat

1d). Nucleolar Cdc2 was colocalized with Cdc13 (Fig. 3C, Stat), suggesting that Cdc2 localizes to the nucleolus in a complex with a B-type cyclin. Cdc2 also colocalized with Clp1 phosphatase, which is localized in the nucleolus during most of the cell cycle and

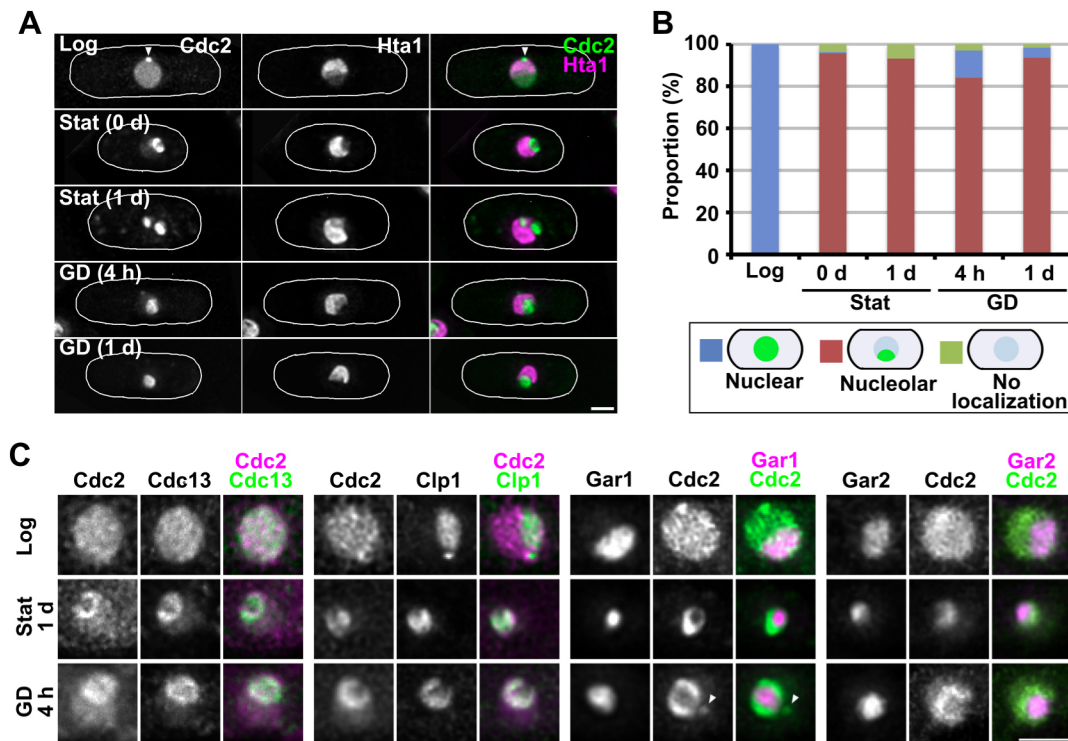


Fig. 3. Changes in Cdc2 localization in stationary phase and after acute glucose depletion. (A) Intracellular localization of Cdc2 and chromosomes (Hta1). White lines indicate cell outlines. An arrowhead indicates SPB localization of Cdc2. Scale bar: 2 μ m. (B) Cdc2 localization patterns. Nuclear, nuclear localization; Nucleolar, nucleolar accumulation; No localization, no obvious intracellular localization. More than 100 cells were examined for each sample. (C) Localization of Cdc2-related or nucleolar proteins. Arrowheads indicate an extra dot in the chromosomal region. Images are representative of more than 10 cells. Scale bar: 2 μ m. Log, log phase cells; Stat, stationary phase cells; GD, GD cells.

eliminates CDK-dependent phosphorylation (Fig. 3C, Stat 1 d), although Cdc2 nucleolar localization was not dependent on Clp1 (data not shown). By contrast, in stationary phase, Cdc2 was not colocalized with the conserved nucleolar proteins, Gar1 and Gar2 (Girard et al., 1993; Gulli et al., 1995), which accumulated in the central nucleolar region (Fig. 3C, Stat 1 d). These observations indicate that the stationary phase nucleolus has at least two distinct regions, a Gar1- and Gar2-enriched central region and a Cdc2- and Clp1-enriched peripheral region. The localization of these proteins was largely similar in GD cells (Fig. 3A–C, GD), although Gar1 and Gar2 often formed one or more extra dots in the chromosomal region (Fig. 3C, GD 4 h, arrowheads). Thus, glucose depletion is the cause of Cdc2 nucleolar accumulation.

The nucleolar localization pattern of Cdc13, Clp1 and Gar2 seen in stationary phase and GD cells was reminiscent of that seen in cells exposed to acute heat stress (Gallardo et al., 2020). We found that Cdc2 also frequently accumulated at the periphery of the nucleolus in cells exposed to 42°C for 20 min (75.8%, $n=95$) (Fig. S3). Furthermore, we found that incubation of cells for 2 h in YES medium containing 0.5 M Mg^{2+} resulted in a similar nucleolar accumulation of Cdc2 together with the cell cycle arrest, albeit with a reduced frequency (29.3%, $n=150$) (Fig. S3). These results suggest that Cdc2 nucleolar accumulation is a common cellular response to environmental stresses.

Stationary phase cells live longer than GD cells in glucose-depleted environments

Our analysis of the GD state indicates that acute glucose depletion induces a state that is similar, but not completely the same, as the stationary phase state. We reasoned that if the purpose of the stationary phase state were to promote cell survival under

nutrient-poor conditions, stationary phase cells should live longer in glucose-free medium than GD cells. To test this hypothesis, stationary phase and GD cells were incubated in YES-Glc medium and their viability over time was compared.

Without medium change, stationary phase cells mostly died within a few days, as reported previously (Fig. 4A) (Zuin et al., 2010). However, when they were transferred to fresh YES-Glc medium, they lived for a longer period, and dilution of the cell density further extended their survival period (Fig. 4A). Medium change- and dilution-dependent extension of cell survival probably results from an increase in the available essential nutrients for each cell given that addition of nutrients other than glucose into the stationary phase culture extended the survival period (Fig. 4B). Thus, stationary phase cells utilize nutrients other than glucose to survive under glucose-depleted conditions. As for stationary phase cells, GD cells lived for a longer period at lower cell density in YES-Glc medium (Fig. 4C). However, their survival time was shorter than that of stationary phase cells at the same cell density (Fig. 4A,C). These results indicate that GD cells lose viability more rapidly than stationary phase cells under glucose-depleted conditions and suggest that GD cells are less resistant to glucose-depleted environments or more rapidly consume essential nutrients compared with stationary phase cells.

Cdc2 activity is required for the establishment of the stationary phase state

Having characterized the stationary phase state, we next investigated the contribution of Cdc2 activity to its establishment by using a *cdc2-L7* temperature-sensitive mutant (Moreno et al., 1989). We found that although *cdc2-L7* cells did not grow at the higher temperature (34°C), they grew at 32°C at a growth rate that was comparable to that of

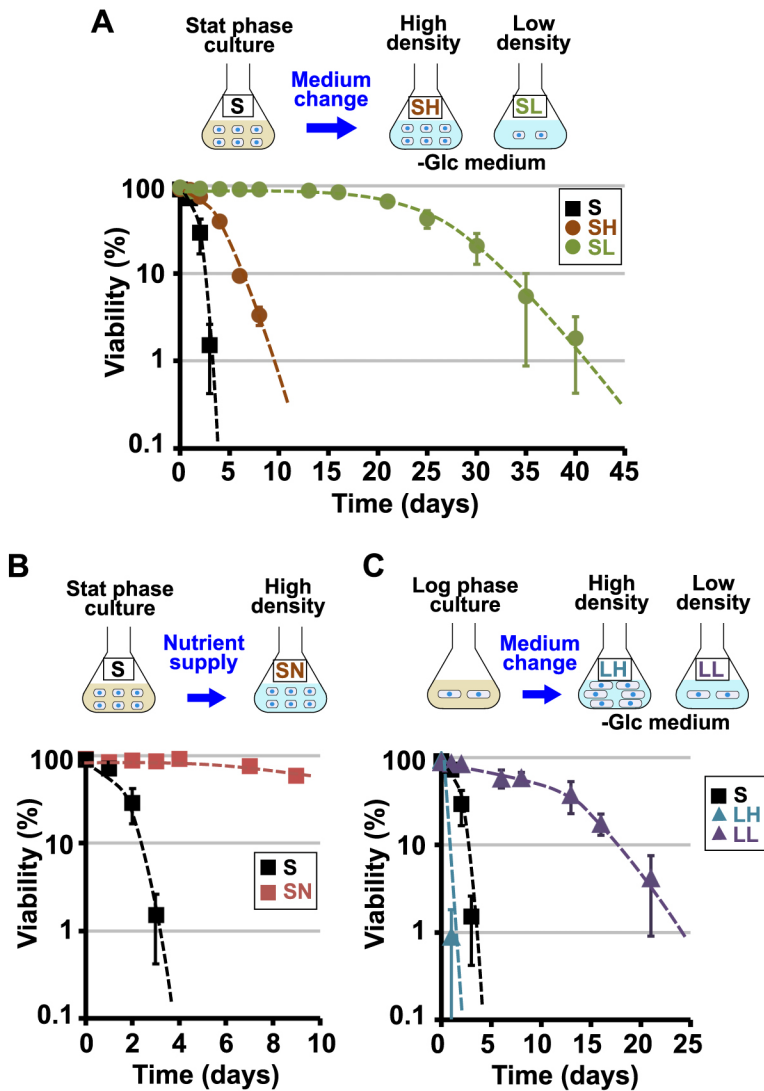


Fig. 4. Viability of stationary phase and GD cells. (A) Changes in viability of stationary phase cells over time. WT cells were grown to stationary phase and further incubated without medium change (S) or after changing the medium to fresh YES-Glc medium (SH and SL). SH, high cell density; SL, low cell density. (B) Changes in cell viability of stationary phase cells after supply of yeast extracts in the culture medium. S, no nutrient supply; SN, with nutrient supply. (C) Changes in viability of GD cells in the YES-Glc medium over time. LH, high cell density; LL, low cell density. The graphs show mean \pm s.e.m. viabilities obtained from more than three independent experiments, and cells were suspended in YES-Glc medium at a concentration of 1.0×10^8 (high cell density) or 5.0×10^6 cells/ml (low cell density). Upper illustrations demonstrate the culture scheme.

wild-type (WT) cells (Fig. 5A,B). However, at 32°C , *cdc2-L7* cells entered stationary phase at lower cell density than WT cells (Fig. 5B, C). Sizes of the cell, the nucleus and the chromosome-occupying space decreased, but were significantly larger compared with those in WT cells (Fig. 5D–F; Figs S4 and S5A). These differences were already evident in log phase and, despite the larger cell and nuclear sizes, there was no significant difference in the N/C ratio between log and stationary phases (Fig. 5G), suggesting that the larger nuclear size results from the larger cell size. Furthermore, the log phase chromosomes more actively fluctuated in *cdc2-L7* cells than in WT cells, and despite a repression in chromosome fluctuation, fluctuation was still elevated in the stationary phase, as demonstrated by an upward shift of the *cdc2-L7* MSD plot of the *ade6* locus and a complete lack of an overlap of their 95% confidence intervals with those of the WT plot (Fig. 5H). The separation frequencies of sister chromatid loci in *cdc2-L7* cells significantly increased in stationary phase compared with WT cells (Fig. 5I). These differences were not evident at 25°C (Figs S4, S5A,B,D–G). Therefore, in the mutant cells at the boundary temperature, Cdc2 activity was reduced to a level that did not inhibit cell cycle progression but caused changes in log and stationary phase states. These results indicate that Cdc2 activity contributes to the establishment of the stationary phase state and suggest that the preceding cell cycle is important for a proper stationary phase state.

We next examined contribution of Cdc2 to the GD state establishment. After acute glucose depletion, nuclear and chromosomal sizes were significantly larger in *cdc2-L7* cells than in WT cells at 32°C , but not at 25°C (Fig. 5E,F; Figs S4, S5C–E,G). However, the N/C ratio was not significantly different (Fig. 5G), suggesting that the larger nuclear size in *cdc2-L7* cells results from their larger cell size. The separation frequencies of sister chromatids were not significantly different from those of WT cells in the *cdc2-L7* cells (Fig. 5I; Figs S4, S5H). To fully elucidate the contribution of Cdc2 to nuclear size reduction, we inhibited Cdc2 activity upon glucose depletion using an analog-sensitive Cdc2 variant (Cdc2-as), whose kinase activity can be inhibited by the ATP analog 3MB-PP1 (Dischinger et al., 2008). Cells containing mCherry-tagged Cdc2-as as the sole Cdc2 were grown, and their Cdc2 activity was inhibited by adding 3MB-PP1 to the culture. After a 10-min treatment, which did not cause any significant changes in nuclear size, cells were transferred to YES-Glc medium containing 3MB-PP1. As a control, cells were treated with DMSO, the solvent for the analog. In the presence of 3MB-PP1, despite some reduction, the nuclear size and the N/C ratio were significantly larger than those seen in the presence of DMSO (Fig. 5J,K; Fig. S4). This result indicates that Cdc2 contributes to nuclear size reduction in response to acute glucose depletion.

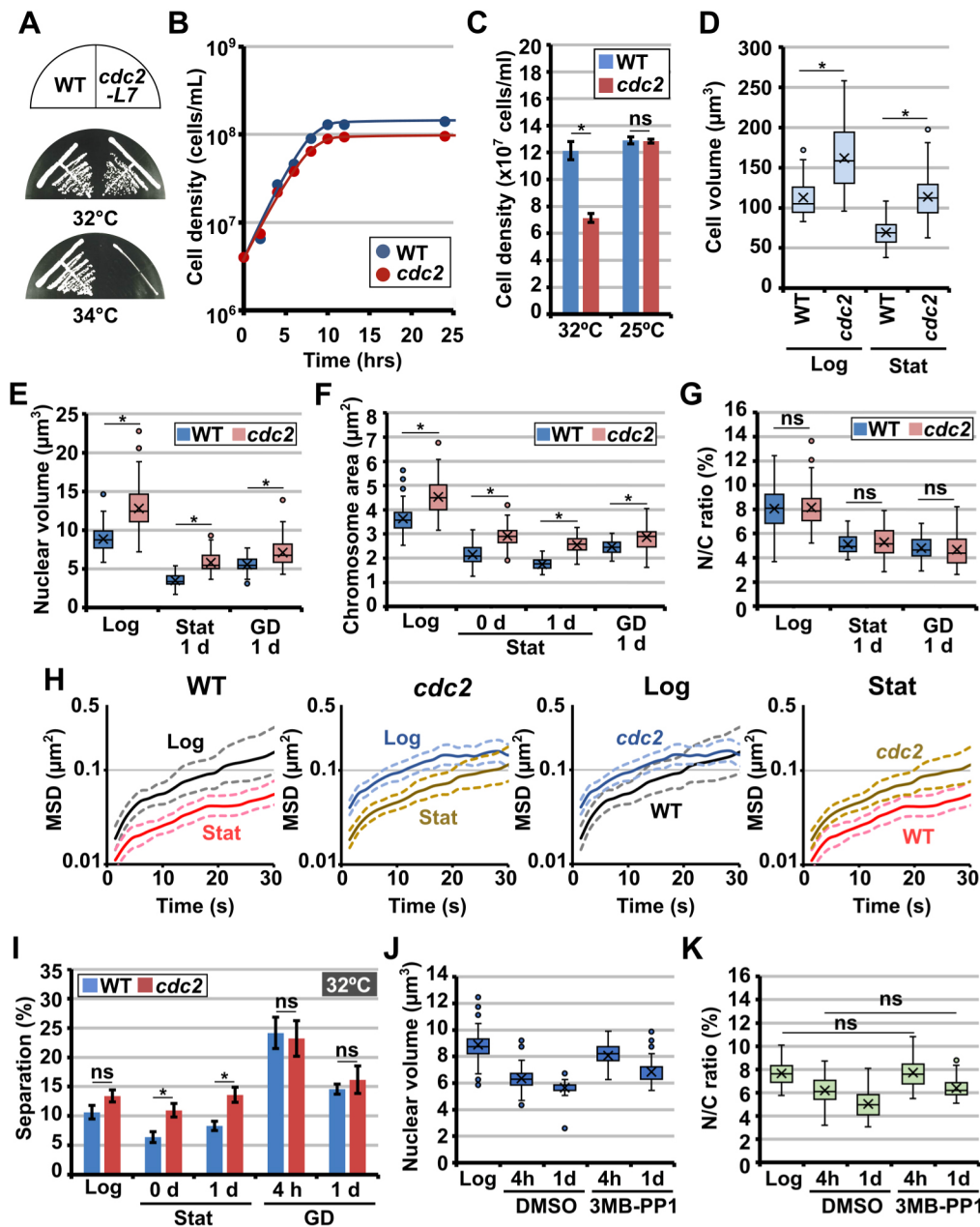


Fig. 5. The effects of *cdc2* temperature-sensitive mutation on the cell state. (A) Growth of *cdc2-L7* and WT cells on YES solid medium at 32°C and 34°C. Image representative of three repeats. (B) Growth curves of WT and *cdc2-L7* cells at 32°C. (C) Cell density of WT and *cdc2-L7* cells in stationary phase. Mean±s.e.m. densities obtained from three independent experiments are shown. * $P < 0.005$. (D) Volumes of WT and *cdc2-L7* cells in log and stationary phases at 32°C. More than 60 cells were examined for each analysis. (E–G) Nuclear volume (E), the area of chromosome-occupying space (F), and the N/C ratio (G) in WT and *cdc2-L7* cells at 32°C. More than 50 cells were examined for each analysis. (H) The MSD plots of the GFP-visualized *ade6* locus in WT and *cdc2-L7* cells at 32°C. Cells in stationary phase for 1 day were analyzed. Dotted lines indicate 95% confidence intervals obtained by the bootstrap method. For plots of WT and *cdc2-L7* cells, more than 8 and 24 cells were examined, respectively. (I) Separation frequencies of sister loci in WT and *cdc2-L7* cells at 32°C. Sister locus separation was examined at the *ade6* locus in more than 100 cells for each analysis, and bars indicate mean±s.e.m. values obtained from three independent experiments. * $P < 0.05$. (J,K) The volume of the nucleus (J) and the N/C ratio (K) in *cdc2-as* GD cells. DMSO: in the presence of 0.1% DMSO; 3MB-PP1: in the presence of 4 μM 3MB-PP1. More than 50 cells were examined for each analysis. In C, G and I, only statistical comparisons between WT and *cdc2-L7* cells are shown. In J and K, only pairwise data sets with a non-significant difference ($P > 0.05$) are shown. All statistical analyses were carried out using the unpaired two-tailed Student's *t*-test, and *P*-values except those in I were corrected by Bonferroni correction (Fig. S4). ns, not significant. For all box and whiskers plots, the horizontal line indicates the median, the box indicates the interquartile range of the data set (IQR), whiskers show the rest of the distribution within 1.5× IQR, circles outside of whiskers show outliers, and the cross indicates the mean value. Log, log phase cells; Stat, stationary phase cells; GD, GD cells.

Cdc2 activity is required for Cdc2 nucleolar accumulation

We next examined whether Cdc2 activity is required for its nucleolar accumulation. Cdc2 kinase activity is negatively regulated

by its phosphorylation at tyrosine 15, and Cdc2 becomes constitutively active and inactive upon replacement of tyrosine 15 with phenylalanine (Cdc2-Y15F) or glutamic acid (Cdc2-Y5E),

respectively (Fig. 6A) (Gould and Nurse, 1989). Cdc2 activity is also abolished by replacement of lysine 33 at the ATP-binding site of the catalytic domain with arginine (Cdc2-KD) (Fig. 6A) (Booher

and Beach, 1986; Hanks et al., 1988). When introduced in the WT background, all of these Cdc2 variants were localized in the nucleus in log phase (Fig. 6B,C). In the stationary phase, Cdc2-Y15F

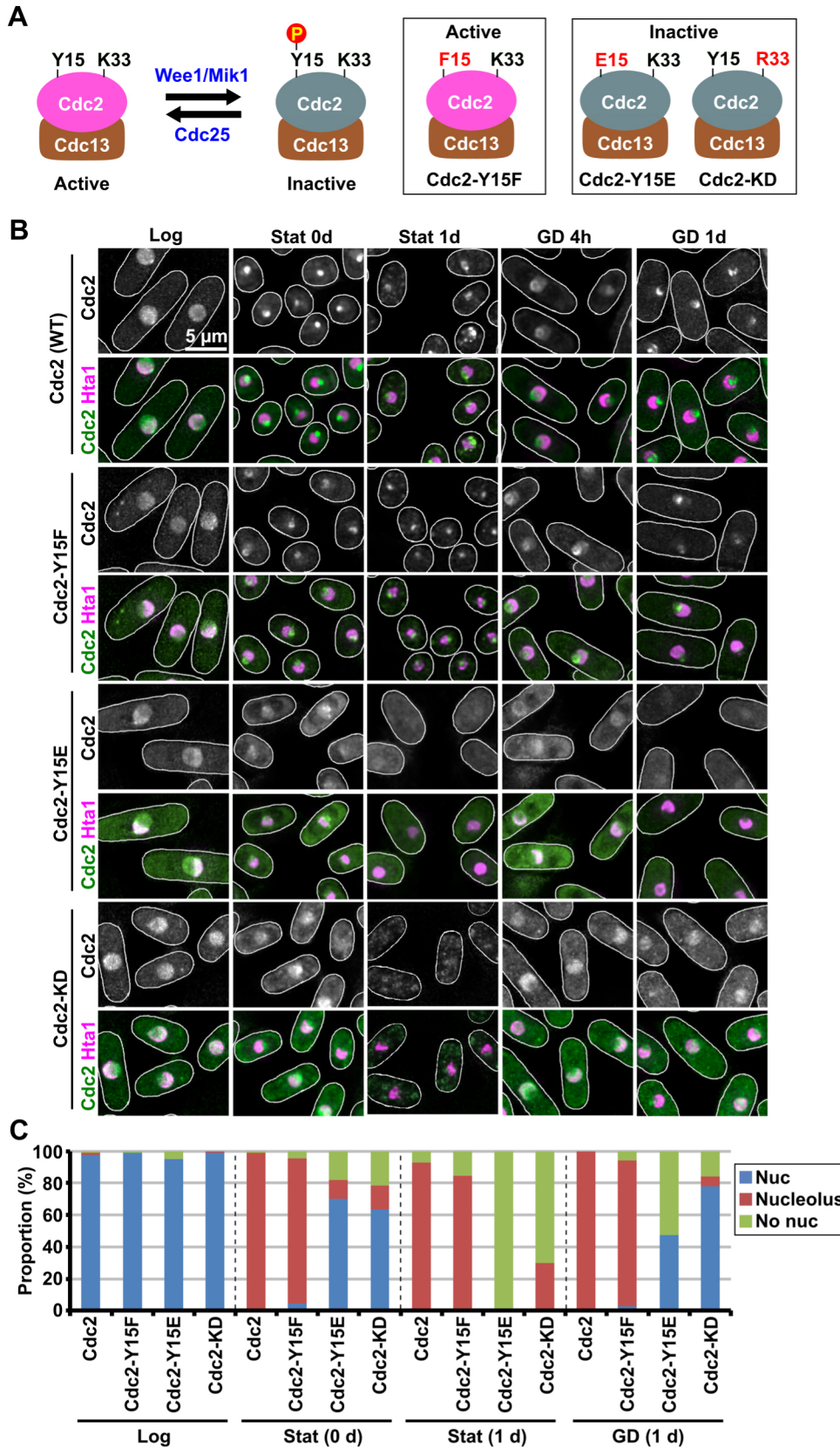


Fig. 6. Defective nucleolar localization of inactive Cdc2 variants. (A) Cdc2 variants used in this study. Mutated amino acids and their residue number are shown. P, phosphorylation. (B) Intracellular localization of Cdc2 variants. Scale bar: 5 μm. (C) Intracellular localization patterns of Cdc2 variants. Graph shows representative Cdc2 localization patterns obtained from one of two replicates. More than 70 cells were examined for each analysis. Nuclear, nuclear localization; Nucleolus, nucleolar accumulation; No nuc, no obvious nuclear localization. Log, log phase cells; Stat, cells in stationary phase for indicated times; GD, GD cells incubated in YES-Glc medium for indicated times.

accumulated in the nucleolus, whereas Cdc2-Y15E or Cdc2-KD often failed to accumulate in the nucleolus and eventually disappeared from the nucleus (Fig. 6B,C). At 1 day after entry into the stationary phase, Cdc2-Y15E mostly failed to localize in the cytoplasm in a granular staining pattern (Fig. 6B). Signal intensities of Cdc2 in the nucleolar region relative to those in the chromosomal region confirmed these localization patterns (Fig. S6A–E). These results indicate that Cdc2 activity is necessary for the nucleolar accumulation of Cdc2 in stationary phase.

We next examined the localization of these Cdc2 variants in GD cells. In GD cells, although Cdc2-Y15F successfully accumulated in the nucleolus, Cdc2-Y15E and Cdc2-KD did not (Fig. 6B,C; Fig. S6A–E). Furthermore, upon acute glucose depletion, mCherry-tagged Cdc2-as, which was localized in the nucleus during log phase, accumulated in the nucleolus in the presence of DMSO but was mostly excluded from the nucleolus in the presence of 3MB-PP1 (Fig. 7). These results indicate that Cdc2 activity is required for Cdc2 nucleolar accumulation in GD cells. Finally, in both stationary phase and GD cells, overall protein levels of WT and mutant forms of Cdc2 were similar and remained unchanged under all conditions, indicating that the frequent lack or weakening of signal seen with inactive Cdc2 variants did not result from Cdc2 degradation (Fig. S6F,G).

Cdc2 activity is required for survival of stationary phase cells under glucose-depleted conditions

We next investigated the requirement of Cdc2 activity for survival of stationary phase and GD cells under glucose-depleted conditions. At 32°C, the viability of *cdc2-L7* cells was comparable to that of WT cells in log phase but decreased more rapidly than that of WT cells in stationary phase (Fig. 8A). The difference was even more striking when stationary phase cells were transferred to fresh

YES-Glc medium (Fig. 8B). The difference in viability was marginal or not significant at 25°C (Fig. 8A,B). These results indicate that Cdc2 activity is required for survival of stationary phase cells under glucose-depleted conditions. We next addressed whether Cdc2 activity is required before and/or after stationary phase entry by temperature shift. No significant differences were observed when cells were incubated at 32°C after entry into stationary phase, whereas viability of *cdc2-L7* cells decreased more rapidly than that of WT cells when cells were incubated at 32°C before and during entry into stationary phase (Fig. 8C). However, when temperature was downshifted after stationary phase entry, a less severe reduction in viability was observed (Fig. 8B,C). This probably reflects the lack of *cdc2*-independent viability reduction at 32°C (13 days after stationary phase entry, the mean±s.e.m. cell viability of WT cells was 93.3±1.3% at 25°C but 67.0±4.2% at 32°C). These results indicate that Cdc2 activity is crucial for cell survival before and/or upon entry into stationary phase, but dispensable after this point.

We then examined the requirement of Cdc2 activity for survival of GD cells. *cdc2-L7* GD cells lost viability more rapidly than WT GD cells at 32°C, but not at 25°C (Fig. 8D). Furthermore, viability of *cdc2-as* GD cells decreased by one-third shortly after transfer to the 3MB-PP-containing YES-Glc medium, although no further decrease was observed, at least for 2 days (Fig. 8E). These results indicate that Cdc2 activity is also crucial for survival of GD cells.

DISCUSSION

The state of stationary phase cells

In this study, we have characterized the stationary phase state in *S. pombe*. By examining the nucleus and chromosomes, we have found several stationary phase-specific cell properties. First, in addition to reduced cell size (Kelkar and Martin, 2015; Yanagida et al., 2011), volumes of the nucleus and chromosome-occupying space are significantly decreased. Second, the transient partial

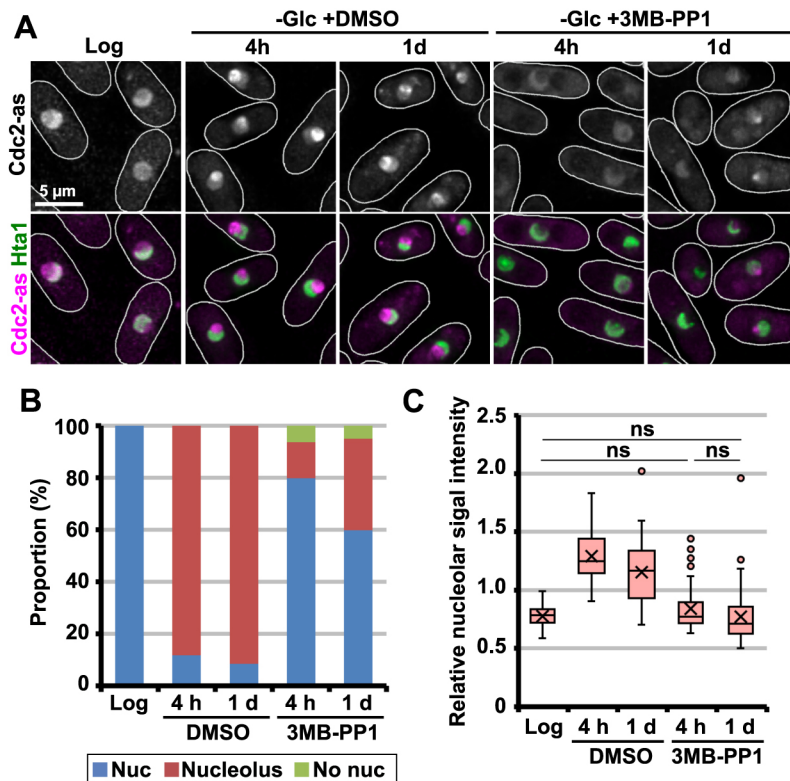


Fig. 7. Inhibition of nucleolar accumulation of Cdc2-as variant by an ATP analog. (A) Intracellular localization of Cdc2-as and Hta1-GFP were grown in YES medium and transferred to YES-Glc medium in the presence of 0.1% DMSO or 5 μ M 3MB-PP1. Scale bar: 5 μ m. (B) Localization patterns of Cdc2-as. More than 120 cells were examined for each analysis. Representative results obtained from one of two independent experiments are shown. (C) Signal intensity of Cdc2 in the nucleolar area relative to that in the chromosomal area. More than 50 cells were examined. Only pairwise data sets with a non-significant difference ($P>0.05$) are shown. Statistical analyses were carried out using the unpaired two-tailed Student's *t*-test, and *P*-values were corrected by the Bonferroni correction (Fig. S6E). For all box and whiskers plots, the horizontal line indicates the median, the box indicates the interquartile range of the data set (IQR), whiskers show the rest of the distribution within 1.5 \times IQR, circles outside of whiskers show outliers, and the cross indicates the mean value. +DMSO, in the presence of DMSO; +3MB-PP1, in the presence of 3MB-PP1.

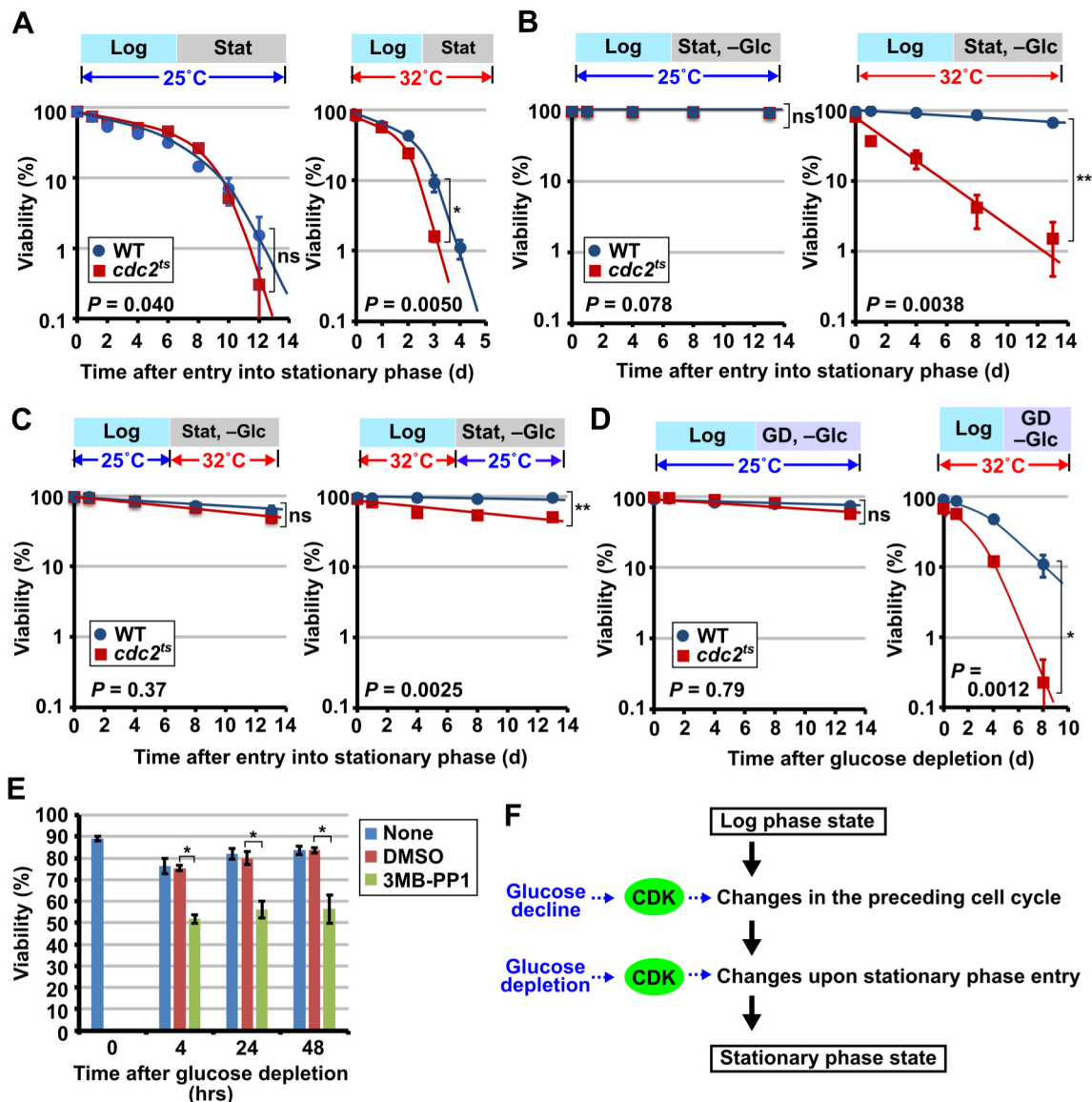


Fig. 8. The role of Cdc2 activity in promoting survival of stationary phase and GD cells. (A–C) Changes in viability of stationary phase *cdc2-L7* mutant and WT cells over time with (B, C) or without medium change (A). In B and C, cells were transferred to fresh YES-Glc medium after entry into stationary phase. In A and B, cells were incubated at the same temperature in both log (Log) and stationary phases (Stat). In C, the incubation temperature was shifted after entry into stationary phase. (D) Changes in viability of GD *cdc2-L7* mutant and WT cells over time. Log phase cells grown in YES medium were transferred to the YES-Glc medium. (E) Effect of 3MB-PP1 on viability of GD cells of *cdc2-as* mutant. Log phase *cdc2-as* cells grown at 30°C were pre-treated with 3MB-PP1 and subsequently incubated in YES-Glc medium containing 4 μ M 3MB-PP1 (3MB-PP1). As a control, cells were treated with DMSO (DMSO). Graphs show the mean \pm s.e.m. viabilities obtained from more than three independent experiments. Log, log phase; Stat, stationary phase, without medium change; Stat -Glc, stationary phase, with medium change; GD -Glc, GD phase. In A to D, upper illustration shows temperature conditions during growth phase. P -values were obtained using the log-rank test, in which the viability data at the previous time points were used when the data were larger than the previous data due to statistical fluctuations. To avoid incorrect statistical evaluation with the non-formal log-rank test, the unpaired two-tailed Student's t -test was also used to analyze the data sets at the last time points (* $P < 0.05$; ** $P < 0.0005$; ns, not significant). (F) Model of the two-step establishment of the stationary phase state.

separation of sister chromatids, which occurs in log phase, is repressed. Third, fluctuation of chromosomes is repressed. Finally, Cdc2 accumulates in the nucleolus together with the B-type cyclin Cdc13.

Size reduction of the nucleus and chromosomes and repression of chromosome fluctuation are probably common characteristics of quiescence, as various quiescent cells exhibit similar changes (Everts et al., 2013; Guidi et al., 2015; Gupta et al., 2012; Joyner et al., 2016; Laporte et al., 2016; Piñon, 1978; Rawlings et al., 2011; Rutledge et al., 2015; Swygert et al., 2019). It is currently unclear whether

repression of sister locus separation is common among quiescent cells, as most other organisms enter quiescence from G1. However, it is possible that the transcription process induces sister locus separation, and that transcription silencing, a common characteristic of quiescence, represses their separation. The restoration of sister locus separation seen at the *ade8* locus might reflect quiescence-associated transcription that occurs around the *ade8* locus after adaptation to nutrient limitation. Likewise, it is unclear whether CDK nucleolar accumulation is a common feature of quiescence. However, nucleolar accumulation of Cdc2 and other regulators is also observed upon exposure to heat or a

high concentration of metal ions (Fig. S2) (Gallardo et al., 2020). Furthermore, in vertebrate cells, upon inhibition of rDNA transcription, CDK2, together with various proteins, accumulates in the nucleolus to form a structure called ‘the nucleolar cap’ (Boulon et al., 2010; Ide et al., 2020; Liu et al., 2000; Reynolds et al., 1964; Scheer and Rose, 1984; Shav-Tal et al., 2005). By contrast, in budding yeast, Cdc28, the sole CDK in that organism, is colocalized with ribonucleoprotein-containing cytoplasmic granules during stationary phase (Shah et al., 2014). These results suggest that CDKs become commonly colocalized with the ribonucleoproteins in response to stress. Perhaps, this colocalization is crucial for the regulation of RNA metabolism. These stationary phase-associated changes are probably essential for cells to survive under glucose-depleted conditions, because when the changes are not fully induced by acute glucose depletion or reduced CDK activity, cells lose viability more rapidly than stationary phase cells in YES-Glc medium.

The establishment of the stationary phase state and survival of stationary phase cells is affected by nutrient availability

We have shown that the GD state resembles, but is not the same as, the stationary phase state. This result suggests that acute glucose depletion is not sufficient for the establishment of the stationary phase state and is consistent with previous results (Klosinska et al., 2011; Yanagida et al., 2011). Given that acute glucose depletion causes immediate cell cycle arrest, these data support the idea that modulation of the preceding cell cycle is required for the stationary phase establishment. Glucose levels gradually decrease in environments, and a low glucose-concentration induces stationary phase-associated phenotypes in cycling cells (Kelkar and Martin, 2015; Klosinska et al., 2011; Pluskal et al., 2011). In addition, Cdc2 nucleolar accumulation occurs upon entry into stationary phase. Taken together, we speculate that the stationary phase state is established in two steps; first, a gradual decline of environmental glucose induces stationary phase-associated changes in cycling cells, and subsequently, glucose depletion induces changes associated with stationary phase entry (Fig. 8F). However, depletion of nutrients other than glucose induces quiescence (Klosinska et al., 2011) and *S. pombe* cells secrete compounds that affect cell growth (Sun et al., 2016). Thus, although glucose depletion is a major trigger of stationary phase, we cannot completely exclude the possibility that depletion or decline of other nutrient(s) and/or the presence of unidentified secreted compounds additionally contribute to stationary phase establishment and that the GD state is different from the stationary phase state due to lack of these additional effects.

We have also found that stationary phase cells utilize nutrients in the medium for their survival and that if appropriate nutrients are supplied, their survival period extends. Therefore, the lifespan of a non-dividing cell, termed the chronological lifespan, changes in different nutritional environments. This suggests that the rapid loss of viability described in some of the previously identified chronological lifespan mutants results from impairment in nutrient utilization or rapid nutrient consumption. It will be important to examine survival periods for various mutants under the same, nutrient-unchangeable conditions to distinguish between death from nutrient starvation and that arising from impairment of stationary phase-specific housekeeping systems.

CDK functions in the establishment of the stationary phase state

Our analysis of *cdc2-L7* mutant demonstrates that CDK is crucial for a proper stationary phase state. In *cdc2-L7* cells, the differences were

already evident in log phase, and nuclear and chromosome size reduction occurred in stationary phase. These observations suggest that the observed improper stationary phase state originates from the improper state of cycling cells and not from impairment in stationary phase-associated changes. Even if so, it is obvious that CDK-dependent regulation of the preceding cell cycle is crucial for a proper stationary phase state. It is also apparent that CDK induces cell size reduction by modulating the preceding cell cycle (Kelkar and Martin, 2015; Petersen and Nurse, 2007; Yanagida et al., 2011). Furthermore, Cdc2 activity is required for Cdc2 nucleolar accumulation and nuclear size reduction upon acute glucose depletion. All these results support the idea that CDK plays a crucial role in stationary phase establishment before and upon stationary phase entry. Our viability analyses of stationary phase and GD cells also provided evidence to support this hypothesis (Fig. 8A–E).

How does CDK contribute to the stationary phase-associated changes? Nuclear size is determined by osmotic force balance, which depends on the ratio of the numbers of osmotically active molecules in the nucleoplasm to that in the cytoplasm (Lemière et al., 2022). The osmotic force balance is constant irrespective of cell size in cycling cells (Lemière et al., 2022), whereas it is markedly changed in stationary phase and GD cells, as shown by a reduction in the N/C ratio. Furthermore, solidification of the cytoplasm occurs in stationary phase and GD cells (Heimlicher et al., 2019; Joyner et al., 2016), which likely increases the osmotic pressure on the nucleus if the gelation is induced by increased hydrophilicity, expressed as a decrease in the Flory–Huggins parameter χ (Strobl, 2007). Therefore, a reduction in the intranuclear molecules and/or cytoplasmic solidification is likely to cause nuclear size reduction. In addition, given that lipid metabolism and membrane flow contribute to nuclear size regulation (Kume et al., 2017, 2019), alteration in the nuclear membrane homeostasis may further contribute to the nuclear size reduction. CDK might induce nuclear size reduction by regulating nuclear transport, cytoplasmic solidification and/or nuclear membrane homeostasis.

A decrease in the chromosome-occupying space might reflect a quiescence-associated chromosome compaction, which likely represses chromosome fluctuation. Upon nitrogen starvation, RNA interference-dependent histone modifications induce heterochromatin formation, resulting in inactivation of transcription (Joh et al., 2016; Roche et al., 2016), and in budding yeast, condensin-dependent intrachromosomal interaction at longer distances increases chromosome compaction and inhibits transcription in stationary phase (Rutledge et al., 2015; Swygert et al., 2019). Given that RNA interference-dependent heterochromatin formation and condensin activity are tightly coupled with the cell cycle (Kloc and Martienssen, 2008; Thadani et al., 2012), CDK might increase chromosome compaction and repress chromosome fluctuation by regulating histone modification and/or condensin activity. CDK might similarly regulate chromosome compaction and fluctuation in cycling cells, accounting for the increase in chromosome size and fluctuation seen in cycling *cdc2-L7* cells. We also cannot exclude the possibility that the chromosome compaction level is coupled with the nuclear size by an uncharacterized molecular mechanism and that CDK changes the chromosome compaction and fluctuation by regulating nuclear size.

Given that the cohesin protein complex establishes sister chromatid cohesion through DNA replication (Blow and Tanaka, 2005; Koshland and Guacci, 2000), CDK likely increases sister chromatid association in response to nutrient decline by regulating

cohesin in the preceding cell cycle, thus repressing sister chromatid separation in stationary phase. In *cdc2-L7* cells, sister chromatid separation could be increased at an undetected level during log phase, resulting in an increase in sister chromatid separation in stationary phase. Supporting this idea, the functions of cohesin regulatory factors are altered in cycling cells under nutrient-limited conditions (Yanagida et al., 2011).

Given that nucleolar CDK accumulation occurs in response to various environmental stresses, CDK must have a common task at the nucleolus in stress responses. Inhibition of rDNA transcription is a common stress response in both quiescent and heat shock-responsive yeast cells (Claypool et al., 2004; Marguerat et al., 2012; Zhao et al., 2016). In addition, CDK inhibits rDNA transcription in mitosis (Heix et al., 1998; Sirri et al., 2002). Given these facts, we speculate that CDK accumulates in the nucleolus to inhibit rDNA transcription. The observed frequent Cdc2 localization to the two distinct regions might correspond to accumulation of Cdc2 at the two rDNA loci adjacent to both telomeres of chromosome III, which promotes transcriptional inhibition. As Gar1 and Gar2 are RNA-binding proteins (Girard et al., 1993; Gulli et al., 1995), it is also likely that these factors form an rRNA-containing stress granule-like structure, which represses rRNA metabolism at the nucleolar center. Alternatively, because cell cycle arrest is a common stress response, CDK might be sequestered at the nucleolus to promote termination of cell cycle progression. Given the requirement of Cdc2 activity for its nucleolar localization, Cdc2 likely executes its task through its phosphorylation-dependent interaction with a nucleolar factor or factors. However, phosphorylation of the nucleolar interactor(s) does not appear to be responsible for this localization, given that inactive Cdc2 variants failed to accumulate in the nucleolus even in the presence of endogenous intact Cdc2. One possibility is that the Cdc2–Cdc13 complex autophosphorylates, promoting the interaction of Cdc2 with the nucleolar factor.

Although CDK is crucial for stationary phase-associated changes, CDK inhibition did not completely prevent the nuclear size reduction and Cdc2 nucleolar accumulation in GD cells (Figs 5J and 7). Thus, CDK is not absolutely required for these changes, and other factors contribute. Many nutrient- and/or stress-responsive kinases including, TOR kinase, PKA, MAPK and AMPK, contribute to the establishment of quiescence and/or survival of quiescent cells (Forte et al., 2019; Gray et al., 2004; Petersen and Nurse, 2007; Yanagida, 2009; Zuin et al., 2010). It is likely that CDK collaborates with these kinases to establish the stationary phase, and even in the absence of CDK activity, these kinases might induce stationary phase-associated phenotypes.

Conclusion

We have shown that CDK actively contributes to the establishment of the stationary phase state in *S. pombe*. It is currently unclear whether CDK actively contributes to quiescence induced by distinct nutrient depletion or in other organisms. This is mainly because CDK inhibition is essential for the establishment of quiescence in all cases (Barbet et al., 1996; Daga et al., 2003; Marescal and Cheeseman, 2020; Matson and Cook, 2017; Moreno-Torres et al., 2015; Pajalunga et al., 2007; Sun and Buttitta, 2017; Tesio and Trumpp, 2011; Valcourt et al., 2012; van Velthoven and Rando, 2019; Velappan et al., 2017; Werner-Washburne et al., 1993; Yanagida, 2009; Zinzalla et al., 2007). However, considering the contribution of CDK to nutrient-dependent cell size control in budding yeast (Turner et al., 2012) and that there is a reduction of CDK activity in the cell cycle preceding quiescence in mammalian cells (Adikes et al., 2020; Arora et al., 2017; Barr et al., 2017; Fan and Meyer, 2021; Spencer et al., 2013), we speculate that the active

contribution of CDKs to establishment of quiescence is common among eukaryotes. Furthermore, colocalization of CDKs with ribonucleoproteins seems to be a conserved stress response among eukaryotes. Understanding the functions of the CDK in stationary phase in *S. pombe* will shed a new light on the fundamental mechanisms underlying the establishment of quiescence in eukaryotes.

MATERIALS AND METHODS

Yeast strains, media and basic genetic methods

Strains and DNA primers used in this study are shown in Tables S1 and S2, respectively. YES and EMM media, and basic genetic techniques used in this study were described previously (Moreno et al., 1991). YES and EMM media contain 3% and 2% (w/v) glucose, respectively. Cells in log or stationary phase were prepared by growing cells to a cell density of $\sim 5 \times 10^6$ or $\sim 1.2 \times 10^8$ cells/ml, respectively, by monitoring cell growth every 2 h. For viability analysis, 110 individual cells were placed on YES solid medium using a thin microneedle under a microscope and incubated at 30°C, and viability was determined by their colony formation. To supply nutrients to the stationary phase culture medium, stationary phase cells were removed from the culture medium by centrifugation, and yeast extract was added to the culture medium at the concentration of 0.5% (w/v). The YE-supplied medium was filter sterilized and the removed cells were resuspended in it.

Flow cytometry analysis of intracellular DNA contents

Intracellular DNA contents were analyzed by flow cytometry as previously described (Matsuhara and Yamamoto, 2016), but with the following modification. Intracellular RNA digestion was carried out using 400 $\mu\text{g/ml}$ RNase A and intracellular DNA content was analyzed using a CytoFLEX flow cytometer (Beckman Coulter, Tokyo, Japan).

Visualization of the nuclear membrane, chromosomes, nucleolar proteins and microtubules

The nuclear membrane was visualized using an integration plasmid, which harbors the GFP-tagged N-terminal portion of the cytochrome C reductase gene, as described previously (Nambu et al., 2022). Chromosomes were visualized using the *htal-mCherry* fusion gene, which was generated by inserting the *mCherry* gene at the *htal* chromosomal locus using a PCR-based method (Bähler et al., 1998; Krawchuk and Wahls, 1999). Cdc13 was visualized using the *cdc13-GFP* fusion gene as described previously (Tatebe and Yanagida, 2000). Clp1 was visualized using an integration plasmid pHM49, which was generated as follows. A genomic DNA fragment encoding the *clp1*⁺ gene together with its promoter and a portion of the pFA6a-GFP(S65T)-kanMX6 plasmid (Bähler et al., 1998), which encodes GFP and the *ADHI* terminator, were amplified by PCR, and these amplified fragments were inserted at the multiple cloning site of pYC36 (Chikashige et al., 2004), yielding pHM49. Gar1 was visualized using an integration plasmid harboring the *gar1-mCherry* gene as described previously (Matsuhara and Yamamoto, 2016). Gar2 was visualized using the *gar2-mCherry* gene obtained from the Yeast Genetic Resource Center Japan. Microtubules were visualized as previously described (Yoshida et al., 2013).

GFP visualization of the chromosome locus

The chromosome locus was visualized using the *lacI/lacO* recognition system, as described previously (Nabeshima et al., 1998; Yamamoto and Hiraoka, 2003), except that a different *lacI* construct was used. An integration plasmid, pMH1, which bears a *lacI* construct lacking the NLS, was generated by inserting a PCR-amplified DNA fragment encoding the GFP-tagged *lac* repressor at the cloning site of pTO2 (Yoshida et al., 2013) together with a PCR-amplified DNA fragment bearing the *nda3* promoter. pMH1 was introduced into cells bearing the *lacO* repeats at the *nhe1*, *ade8* or *ade6* chromosomal locus.

Construction of *cdc2* variants

WT Cdc2 was visualized using the endogenous *cdc2*⁺ gene fused with the *GFP* gene (a gift from Dr Hiroshi Murakami, Department of Biological

Sciences, Chuo University, Japan) or using integration plasmids, pYN9 and pYN11, which bear *cdc2*⁺-GFP and *cdc2*⁺-mCherry fusion genes, respectively. pYN9 and pYN11 were generated as follows. Genomic and complementary DNA fragments encoding the *cdc2* promoter and the *cdc2*⁺ gene, respectively, were amplified by PCR and inserted in front of the *mCherry* gene on an integration plasmid pHM4 (Yoshida et al., 2013), yielding pYN11. The PCR-amplified DNA fragments encoding the *cdc2* promoter and CDS were also inserted at the cloning site of an integration plasmid, pTO2 (Yoshida et al., 2013) together with a PCR-amplified portion of a plasmid DNA, pFA6a-GFP(S65T)-kanMX6 (Bähler et al., 1998), encoding GFP(S65T) and the *ADHI* terminator, yielding pYN9. The endogenous *cdc2*⁺ gene was deleted in cells expressing the *cdc2*⁺-GFP fusion using a PCR-based method (Bähler et al., 1998; Krawchuk and Wahls, 1999).

The *cdc2-as* mutant protein tagged with mCherry was introduced into cells using the integration plasmid pYN14. pYN14 was generated by introducing the corresponding mutation at the *cdc2*⁺-mCherry gene on pYN11 (see above), using the KOD-Plus-Mutagenesis Kit (TOYOBO, Osaka, Japan). The *cdc2-Y15F*, *cdc2-Y15E*, or *cdc2-KD* mutant protein tagged with GFP was introduced into cells using the integration plasmids, pYN7, pYN8 or pYN10, respectively. pYN7, pYN8 and pYN10 were generated by introducing the corresponding mutation at the *cdc2*⁺-GFP gene on pYN9 (see above), using the KOD-Plus-Mutagenesis Kit.

Quantification of area and volume of the cell, the nucleus and the chromosome-occupying space, and analysis of sister locus separation and intracellular localization of various molecules

Given that placing cells between a slide glass and a coverslip caused rapid changes in the nuclear shape and intracellular localization of Cdc2 during observation, cells were observed using the following alternative method. Log phase cells were suspended in EMM medium, and stationary phase and GD cells were suspended in EMM-Glc medium. When cells were treated with chemicals, the cells were suspended in the medium containing the appropriate compound. ~20 μ l of the cell suspension was placed on a 40 \times 50 mm coverslip (Matsunami Glass Ind., Ltd., Osaka, Japan) coated with 5 mg/ml lectin (Sigma-Aldrich Japan, Co., Tokyo, Japan). The cells were observed using an IX71 inverted microscope equipped with a cooled charge-coupled device camera (CoolSNAP-HQ2; Nippon Roper Co. Ltd., Tokyo, Japan) and a 60 \times /1.42 NA or 100 \times /1.40 NA Plan Apo oil-immersion objective lens (Olympus, Tokyo, Japan). Images of the nuclear envelope, chromosomes, or Cdc2 were taken at 11 or 20 focal planes spaced at 0.3 μ m intervals. The resultant images were processed by deconvolution and analyzed using the MetaMorph (version 7) (Molecular Devices Japan, Tokyo, Japan) or ImageJ software (Schneider et al., 2012).

Cell volume was calculated using the Pombe Measurer ImageJ plugin (http://www.columbia.edu/~zz2181/Pombe_Measurer.html; Pino et al., 2021). Nuclear area was determined by fitting an ellipse to the nuclear envelope on one section that showed the clearest envelope image. The nuclear volume was determined by regarding the nucleus as a spheroid with the semi-axis lengths, *a*, *b*, and (*a+b*)/2, where *a* and *b* are the lengths of the semi-axes of the fitted ellipse. Chromosome area was determined using the chromosomal region obtained from the binarized image of chromosomes in the two-dimensional projection formed from the 11 sections. Sister locus separation and intracellular localization of various molecules were analyzed in the two-dimensional projection.

The relative intensity of Cdc2 signal in the nucleolar region to that in the chromosomal region was determined as follows. Each deconvolved image set was combined to form a quantitative projection using an additive image projecting method. Then, the sums of the Cdc2 signal intensities in regions of the nucleus and chromosomes were obtained by subtracting the background signals. The total signal intensity in the nucleolar region was obtained by subtracting the total chromosomal signal intensity from the total nuclear intensity. The relative intensity of the nucleolar signal was determined using the obtained nucleolar and chromosomal signal intensities per area. Note that the relative nucleolar signal intensity was underestimated in this analysis given that the nucleolar region partially overlapped with the chromosomal region in the two-dimensional projection due to the shape and the positioning of the nucleolus.

Analysis of chromosome fluctuation

Cells containing the GFP-visualized locus were transferred to EMM (log phase cells) or EMM-Glc medium (stationary phase cells or log phase cells exposed to acute glucose starvation). Approximately 20 μ l of the cell suspension was placed on the bottom of 35 mm glass-bottom dishes (Matsunami Glass Ind., Ltd., Osaka, Japan) coated with 5 mg/ml lectin. Time-lapse images of the visualized locus in these cells were collected at three focal planes spaced at 0.4 μ m intervals every 1.5 s using an IX71 inverted microscope equipped with a cooled charge-coupled device camera and a 100 \times /1.40 NA Plan Apo oil-immersion objective lens (Olympus, Tokyo, Japan). To minimize each acquisition time, the area captured was less than 800 pixels in size and an exposure time of less than 90 m second was used. During collection of time-lapse images, the cells were kept at 25°C. The resultant images were processed by deconvolution using MetaMorph software, and the three-dimensional coordinate of the GFP-visualized chromosome locus was then determined at each time point using a multi-dimensional motion analysis module. When the visualized sister loci were separated, the coordinate of their midpoint was used for analysis. The obtained coordinates were used to plot MSD plots and their confidence intervals were statistically evaluated. The basic bootstrap method (Davison and Hinkley, 1997) was used to evaluate the confidence intervals, in order to correct for differences in time length of the coordinate data, as previously described (Wakiya et al., 2021). A brief description of the statistical method is given below.

Each data set contains several time series corresponding to different cells from the same strain. Let *S* be the number of cells in the data set under consideration, and let (*x*^(*n*)(*i*), *y*^(*n*)(*i*), *z*^(*n*)(*i*)) be the three-dimensional coordinate of the GFP-visualized chromosome locus of the *n*-th cell at time *i* Δ *t*. Here, *n*=1, 2, ..., *S* labels the individual cells contained in the data set, *i* is an integer, and Δt is the time interval where $\Delta t = 1.5$ s as explained above. Then, the square displacement (SD) from time *i* Δ *t* to (*i*+*j*) Δ *t* is

$$SD^{(n)}(i, i+j) = \left(x^{(n)}(i+j) - x^{(n)}(i) \right)^2 + \left(y^{(n)}(i+j) - y^{(n)}(i) \right)^2 + \left(z^{(n)}(i+j) - z^{(n)}(i) \right)^2. \quad (1)$$

The MSD is the average of Eqn 1 over all the time points and cells:

$$MSD(j\Delta t) = \frac{\sum_{n=1}^S \sum_{i=1}^{L_n-j} SD^{(n)}(i, i+j)}{\sum_{n=1}^S (L_n - j)}, \quad (2)$$

where *L_n* is the length of the time series, which can be different for different *n*.

The confidence intervals for the estimated MSD were evaluated by the basic bootstrap method (Davison and Hinkley, 1997). Re-sampling of the samples of the *S* cells is performed, which we denote by {*n*₁^{*}, *n*₂^{*}, ..., *n*_{*S*}^{*}}, where the numbers *n*_{*k*}^{*} (*k* = 1, 2, ..., *S*) are randomly sampled from {1, 2, ..., *S*} with replacement. The estimation of the MSD by this re-sampled set is given, corresponding to Eqn 2, by:

$$MSD^*(j\Delta t) = \frac{\sum_{k=1}^S \sum_{i=1}^{L_{n_k^*}-j} SD^{(n_k^*)}(i, i+j)}{\sum_{k=1}^S (L_{n_k^*} - j)}, \quad (3)$$

where * denotes the estimates made by using the re-sampled data set. Each re-sampled data set gives a re-sampled estimate MSD*(*j* Δ *t*). The re-sampling is then repeated *R*₁ times, with *R*₁ being a sufficiently large number. This produces a set of *R*₁ values of MSD*(*j* Δ *t*), giving a distribution of MSD*(*j* Δ *t*).

The following transformation is introduced to keep the positivity in the later estimated confidence interval:

$$Z = \log(MSD(j\Delta t)), \quad (4)$$

and similarly *Z*^{*}=log(MSD*(*j* Δ *t*)). The variable *Z* has one-to-one correspondence with MSD(*j* Δ *t*). Let *a*_{*q*}^{*} be such a value that the probability that we have *Z*^{*} \leq *Z* + *a*_{*q*}^{*} is equal to *q*. Then, the confidence region for the true value ζ of *Z* with confidence level *q*,

where we take $1-2\alpha=0.95$, is given by:

$$z - a_{1-\alpha}^* < \zeta < z - a_{\alpha}^* \quad (5)$$

where z is the value of Z obtained using the original data set. To estimate a_q^* , the R_1 re-sampled values $z_1^*, z_2^*, \dots, z_{R_1}^*$ of Z^* are used. These are re-ordered as $z_{(1)}^* \leq z_{(2)}^* \leq \dots \leq z_{(R_1)}^*$. The estimate for a_q^* is then given by $a_q^* = z_{(R_1+1)q}^* - z$. From Eqn 5, the backward transformation to MSD through Eqn 4 gives the confidence interval for MSD($j\Delta t$). In practice, $R_1=5000$ was taken for the number of re-samplings.

Inhibition of Cdc2-as kinase activity using 3MB-PP1 upon acute glucose depletion

Cells containing mCherry-tagged Cdc2-as were grown in YES medium to log phase cell density at 30°C. Cdc2 kinase activity was inhibited by addition of 1:1000 culture volume of 3MB-PP1 stock solution (4 or 5 mM) (Funakoshi, Tokyo, Japan) to the culture and incubation for 10 min with shaking. The cells were then suspended in YES-Glc medium containing 4 or 5 μ M 3MB-PP1 after washing twice with the same medium and further incubated at 30°C. As a control, DMSO was used instead of 3MB-PP1. Note that no differences were detected in *cdc2-as* cells treated with 4 or 5 μ M 3MB-PP1.

Numerical simulation of chromosome fluctuation with spatial confinement

A chromosomal locus was regarded as a particle diffusing in a space surrounded by a spherical wall representing the nuclear envelop. The time step of the simulation was taken to be $\Delta t=0.5$ s. Correlated random numbers were generated to make the displacement of the particle at each step. The statistics of the random displacement is such that $\text{MSD}(t) \propto t^\alpha$, where the exponent is set to be $\alpha=0.67$ in order to reproduce the experimental results. Generation of correlated random numbers was carried out using the Fourier transformation method (Berkowitz et al., 1983). When the particle hits the wall, it is reflected elastically. The radius R_{nuc} of the spherical wall is set to be $R_{\text{nuc}}=1.272 \mu\text{m}$ and $0.856 \mu\text{m}$, obtained from the observed nuclear volumes for the log and stationary phases, respectively. For each nucleus size, 1000 trajectories each with 2^{16} steps were generated, and their statistical average was taken to calculate MSD.

Protein analysis by western blotting

For western blotting analysis of proteins, $\sim 5 \times 10^7$ and $\sim 2 \times 10^8$ cells were collected for log and stationary phase cells, respectively. The cells were washed twice with ice-cold STOP buffer (150 mM NaCl, 50 mM NaF, 1 mM NaN_3 , 10 mM EDTA, pH 8.0) and stored at -80°C until use. The cells were suspended in 20 μ l or 50 μ l water for log phase or stationary phase cells, respectively, and the cell suspension was immediately heated at 100°C for 5 min. Subsequently the suspension was mixed with twice the volume of urea buffer (8 M urea, 4% SDS, 1 mM DTT and 120 mM Tris-HCl pH 7.4). The cells were then disrupted using glass beads and the bead cell disrupter (MagNA Lyser, Nippon Genetic). A portion of the cell extract was used for protein concentration analysis with a BCA protein assay kit (Thermo Fisher Scientific, Tokyo, Japan), and the rest of the extract was mixed with an equal volume of $2 \times$ SDS sample buffer and heated at 100°C for 3 min for protein extraction. After cell debris removal by centrifugation (22,140 g for 15 min), the cell extract containing 40 μ g protein was loaded for each sample onto a 10% SDS-PAGE gel. After electrophoresis, the proteins were detected by western blotting using the following antibodies: mouse monoclonal anti-PSTAIR antibody (1:50,000; P7962; lot no: 090M4829; Sigma-Aldrich), mouse anti-GFP antibody (1:3000; clones 7.1 and 13.1; cat. no: 11 814 460 001; Roche Diagnostics), and mouse monoclonal anti- α -tubulin antibody (1:40,000; clone B-5-1-2; product no: T 5168; Sigma-Aldrich).

Acknowledgements

We are grateful to Tomomi Kato, Yukina Saitoh, Sayaka Yokota, Momoka Ishida, Kenta Sato, Aya Yamaguchi and Sadia Afrin for their contribution to the initial stage of this study; Hirota Matsuhara for constructing plasmid pHM49; Hiroshi Murakami and the Yeast Genetic Resource Center for strains; and Takashi Ushimaru for the use of the bead cell disrupter. We are also grateful to Masahiro Uritani, Takashi Ushimaru and Yoko Kimura for helpful discussions, and Yoko Kimura and Hiroshi

Murakami for critical reading of the manuscript and helpful comments. Intracellular DNA contents were analyzed using the flow cytometer at Shizuoka University Research Institute of Green Science and Technology.

Competing interests

The authors declare no competing or financial interests.

Author contributions

Conceptualization: A.Y.; Validation: S.K., A.Y.; Formal analysis: S.K., A.Y.; Investigation: M.H., Y.K., Y.N., K.Y., K.K., J.-W.C., S.S.; Writing - original draft: S.K., A.Y.; Writing - review & editing: S.K., A.Y.; Supervision: A.Y.; Project administration: A.Y.

Funding

This research received no specific grant from any funding agency in the public, commercial or not-for-profit sectors.

Data availability

All relevant data can be found within the article and its supplementary information.

Peer review history

The peer review history is available online at <https://journals.biologists.com/jcs/lookup/doi/10.1242/jcs.260727.reviewer-comments.pdf>

References

- Adikes, R. C., Kohrman, A. Q., Martinez, M. A. Q., Palmisano, N. J., Smith, J. J., Medwig-Kinney, T. N., Min, M., Sallee, M. D., Ahmed, O. B., Kim, N. et al. (2020). Visualizing the metazoan proliferation-quiescence decision in vivo. *eLife* **9**, e63265. doi:10.7554/eLife.63265
- Arora, M., Moser, J., Phadke, H., Basha, A. A. and Spencer, S. L. (2017). Endogenous replication stress in mother cells leads to quiescence of daughter cells. *Cell Rep.* **19**, 1351-1364. doi:10.1016/j.celrep.2017.04.055
- Bähler, J., Wu, J.-Q., Longtine, M. S., Shah, N. G., Mckenzie, III, A., Steever, A. B., Wach, A., Philippsen, P. and Pringle, J. R. (1998). Heterologous modules for efficient and versatile PCR-based gene targeting in *Schizosaccharomyces pombe*. *Yeast* **14**, 943-951. doi:10.1002/(SICI)1097-0061(199807)14:10<943::AID-YEA292>3.0.CO;2-Y
- Barbet, N. C., Schneider, U., Helliwell, S. B., Stansfield, I., Tuite, M. F. and Hall, M. N. (1996). TOR controls translation initiation and early G1 progression in yeast. *Mol. Biol. Cell* **7**, 25-42. doi:10.1091/mbc.7.1.25
- Barr, A. R., Cooper, S., Heldt, F. S., Butera, F., Stoy, H., Mansfeld, J., Novák, B. and Bakal, C. (2017). DNA damage during S-phase mediates the proliferation-quiescence decision in the subsequent G1 via p21 expression. *Nat. Commun.* **8**, 14728. doi:10.1038/ncomms14728
- Berkowitz, M., Morgan, J. D. and Mccammon, J. A. (1983). Generalized Langevin dynamics simulations with arbitrary time-dependent memory kernels. *J. Chem. Phys.* **78**, 3256. doi:10.1063/1.445244
- Blow, J. J. and Tanaka, T. U. (2005). The chromosome cycle: coordinating replication and segregation. *EMBO Rep.* **6**, 1028-1034. doi:10.1038/sj.embor.7400557
- Bojsen, R., Regenber, B. and Folkesson, A. (2017). Persistence and drug tolerance in pathogenic yeast. *Curr. Genet.* **63**, 19-22. doi:10.1007/s00294-016-0613-3
- Booher, R. and Beach, D. (1986). Site-specific mutagenesis of *cdc2+*, a cell cycle control gene of the fission yeast *Schizosaccharomyces pombe*. *Mol. Cell. Biol.* **6**, 3523-3530. doi:10.1128/MCB.6.10.3523
- Borst, P. (2012). Cancer drug pan-resistance: pumps, cancer stem cells, quiescence, epithelial to mesenchymal transition, blocked cell death pathways, persists or what? *Open Biol.* **2**, 120066. doi:10.1098/rsob.120066
- Boulon, S., Westman, B. J., Hutten, S., Boisvert, F.-M. and Lamond, A. I. (2010). The nucleolus under stress. *Mol. Cell* **40**, 216-227. doi:10.1016/j.molcel.2010.09.024
- Bregues, M., Teixeira, D. and Parker, R. (2005). Movement of eukaryotic mRNAs between polysomes and cytoplasmic processing bodies. *Science* **310**, 486-489. doi:10.1126/science.1115791
- Broach, J. R. (2012). Nutritional control of growth and development in yeast. *Genetics* **192**, 73-105. doi:10.1534/genetics.111.135731
- Chikashige, Y., Kurokawa, R., Haraguchi, T. and Hiraoka, Y. (2004). Meiosis induced by inactivation of Pat1 kinase proceeds with aberrant nuclear positioning of centromeres in the fission yeast *Schizosaccharomyces pombe*. *Genes Cells* **9**, 671-684. doi:10.1111/j.1356-9597.2004.00760.x
- Claypool, J. A., French, S. L., Johzuka, K., Eliason, K., Vu, L., Dodd, J. A., Beyer, A. L. and Nomura, M. (2004). Tor pathway regulates Rm3p-dependent recruitment of yeast RNA polymerase I to the promoter but does not participate in alteration of the number of active genes. *Mol. Biol. Cell* **15**, 946-956. doi:10.1091/mbc.e03-08-0594

- Cole, J. J.** (1999). Aquatic microbiology for ecosystem scientists: new and recycled paradigms in ecological microbiology. *Ecosystems* **2**, 215-225. doi:10.1007/s100219900069
- Daga, R. R., Bolaños, P. and Moreno, S.** (2003). Regulated mRNA stability of the Cdk inhibitor Rum1 links nutrient status to cell cycle progression. *Curr. Biol.* **13**, 2015-2024. doi:10.1016/j.cub.2003.10.061
- Davison, A. C. and Hinkley, D. V.** (1997). *Bootstrap Methods and their Application*. Cambridge University Press.
- De Virgilio, C.** (2012). The essence of yeast quiescence. *FEMS Microbiol. Rev.* **36**, 306-339. doi:10.1111/j.1574-6976.2011.00287.x
- Decottignies, A., Zarzov, P. and Nurse, P.** (2001). In vivo localisation of fission yeast cyclin-dependent kinase cdc2p and cyclin B cdc13p during mitosis and meiosis. *J. Cell Sci.* **114**, 2627-2640. doi:10.1242/jcs.114.14.2627
- Ding, D.-Q., Tomita, Y., Yamamoto, A., Chikashige, Y., Haraguchi, T. and Hiraoka, Y.** (2000). Large-scale screening of intracellular protein localization in living fission yeast cells by the use of a GFP-fusion genomic DNA library. *Genes Cells* **5**, 169-190. doi:10.1046/j.1365-2443.2000.00317.x
- Ding, D.-Q., Yamamoto, A., Haraguchi, T. and Hiraoka, Y.** (2004). Dynamics of homologous chromosome pairing during meiotic prophase in fission yeast. *Dev. Cell* **6**, 329-341. doi:10.1016/S1534-5807(04)00059-0
- Dischinger, S., Krapp, A., Xie, L., Paulson, J. R. and Simanis, V.** (2008). Chemical genetic analysis of the regulatory role of Cdc2p in the *S. pombe* septation initiation network. *J. Cell Sci.* **121**, 843-853. doi:10.1242/jcs.021584
- Evertts, A. G., Manning, A. L., Wang, X., Dyson, N. J., Garcia, B. A. and Collier, H. A.** (2013). H4K20 methylation regulates quiescence and chromatin compaction. *Mol. Biol. Cell* **24**, 3025-3037. doi:10.1091/mbc.e12-07-0529
- Faire, M., Skillern, A., Arora, R., Nguyen, D. H., Wang, J., Chamberlain, C., German, M. S., Fung, J. C. and Laird, D. J.** (2015). Follicle dynamics and global organization in the intact mouse ovary. *Dev. Biol.* **403**, 69-79. doi:10.1016/j.ydbio.2015.04.006
- Fan, Y. and Meyer, T.** (2021). Molecular control of cell density-mediated exit to quiescence. *Cell Rep.* **36**, 109436. doi:10.1016/j.celrep.2021.109436
- Forté, G. M., Davie, E., Lie, S., Franz-Wachtel, M., Ovens, A. J., Wang, T., Oakhill, J. S., Maček, B., Hagan, I. M. and Petersen, J.** (2019). Import of extracellular ATP in yeast and man modulates AMPK and TORC1 signalling. *J. Cell Sci.* **132**, jcs223925. doi:10.1242/jcs.223925
- Gallardo, P., Real-Calderón, P., Flor-Parra, I., Salas-Pino, S. and Daga, R. R.** (2020). Acute heat stress leads to reversible aggregation of nuclear proteins into nucleolar rings in fission yeast. *Cell Rep.* **33**, 108377. doi:10.1016/j.celrep.2020.108377
- Girard, J.-P., Caizergues-Ferrer, M. and Lapeyre, B.** (1993). The SpGAR1 gene of *Schizosaccharomyces pombe* encodes the functional homologue of the snoRNP protein GAR1 of *Saccharomyces cerevisiae*. *Nucleic Acids Res.* **21**, 2149-2155. doi:10.1093/nar/21.9.2149
- Gould, K. L. and Nurse, P.** (1989). Tyrosine phosphorylation of the fission yeast *cdc2+* protein kinase regulates entry into mitosis. *Nature* **342**, 39-45. doi:10.1038/342039a0
- Gray, J. V., Petsko, G. A., Johnston, G. C., Ringe, D., Singer, R. A. and Werner-Washburne, M.** (2004). "Sleeping beauty": quiescence in *Saccharomyces cerevisiae*. *Microbiol. Mol. Biol. Rev.* **68**, 187-206. doi:10.1128/MMBR.68.2.187-206.2004
- Guidi, M., Ruault, M., Marbouty, M., Loïdode, I., Cournac, A., Billaudeau, C., Hocher, A., Mozziconacci, J., Koszul, R. and Taddei, A.** (2015). Spatial reorganization of telomeres in long-lived quiescent cells. *Genome Biol.* **16**, 206. doi:10.1186/s13059-015-0766-2
- Gulli, M.-P., Girard, J.-P., Zabetakis, D., Lapeyre, B., Melese, T. and Caizergues-Ferrer, M.** (1995). gar2 is a nucleolar protein from *Schizosaccharomyces pombe* required for 18S rRNA and 40S ribosomal subunit accumulation. *Nucleic Acids Res.* **23**, 1912-1918. doi:10.1093/nar/23.11.1912
- Gupta, S., Marcel, N., Talwar, S., Garg, M., R. I., Perumalsamy, L. R., Sarin, A. and Shivashankar, G. V.** (2012). Developmental heterogeneity in DNA packaging patterns influences T-Cell activation and transmigration. *PLoS ONE* **7**, e43718. doi:10.1371/journal.pone.0043718
- Hanks, S. K., Quinn, A. M. and Hunter, T.** (1988). The protein kinase family: conserved features and deduced phylogeny of the catalytic domains. *Science* (1979) **241**, 42-52. doi:10.1126/science.3291115
- Hayles, J. and Nurse, P.** (2018). Introduction to fission yeast as a model system. *Cold Spring Harb. Protoc.* **2018**, pdb.top079749. doi:10.1126/science.3291115
- Heimlicher, M. B., Bächler, M., Liu, M., Ibeneche-Nnewiwe, C., Florin, E.-L., Hoenger, A. and Brunner, D.** (2019). Reversible solidification of fission yeast cytoplasm after prolonged nutrient starvation. *J. Cell Sci.* **132**, jcs231688. doi:10.1242/jcs.231688
- Heix, J., Vente, A., Voit, R., Budde, A., Michaelidis, T. M. and Grummt, I.** (1998). Mitotic silencing of human rRNA synthesis: Inactivation of the promoter selectivity factor SL1 by cdc2/cyclin B-mediated phosphorylation. *EMBO J.* **17**, 7373-7381. doi:10.1093/emboj/17.24.7373
- Herman, P. K.** (2002). Stationary phase in yeast. *Curr. Opin. Microbiol.* **5**, 602-607. doi:10.1016/S1369-5274(02)00377-6
- Ide, S., Imai, R., Ochi, H. and Maeshima, K.** (2020). Transcriptional suppression of ribosomal DNA with phase separation. *Sci. Adv.* **6**, eabb5953. doi:10.1126/sciadv.abb5953
- Joh, R. I., Khanduja, J. S., Calvo, I. A., Mistry, M., Palmieri, C. M., Savol, A. J., Ho Sui, S. J., Sadreyev, R. I., Aryee, M. J. and Motamedi, M.** (2016). Survival in quiescence requires the euchromatic deployment of Ctr4/SUV39H by Argonaute-associated small RNAs. *Mol. Cell* **64**, 1088-1101. doi:10.1016/j.molcel.2016.11.020
- Joyner, R. P., Tang, J. H., Helenius, J., Dultz, E., Brune, C., Holt, L. J., Huet, S., Müller, D. J. and Weis, K.** (2016). A glucose-starvation response regulates the diffusion of macromolecules. *eLife* **5**, e09376. doi:10.7554/eLife.09376
- Kelkar, M. and Martin, S. G.** (2015). PKA antagonizes CLASP-dependent microtubule stabilization to re-localize Pom1 and buffer cell size upon glucose limitation. *Nat. Commun.* **6**, 8445. doi:10.1038/ncomms9445
- Kloc, A. and Martienssen, R.** (2008). RNAi, heterochromatin and the cell cycle. *Trends Genet.* **24**, 511-517. doi:10.1016/j.tig.2008.08.002
- Klosinska, M. M., Crutchfield, C. A., Bradley, P. H., Rabinowitz, J. D. and Broach, J. R.** (2011). Yeast cells can access distinct quiescent states. *Genes Dev.* **25**, 336-349. doi:10.1101/gad.2011311
- Koshland, D. E. and Guacci, V.** (2000). Sister chromatid cohesion: the beginning of a long and beautiful relationship. *Curr. Opin. Cell Biol.* **12**, 297-301. doi:10.1016/S0955-0674(00)00092-2
- Krawchuk, M. D. and Wahls, W. P.** (1999). High-efficiency gene targeting in *Schizosaccharomyces pombe* using a modular, PCR-based approach with long tracts of flanking homology. *Yeast* **15**, 1419-1427. doi:10.1002/(SICI)1097-0061(19990930)15:13<1419::AID-YEA466>3.0.CO;2-Q
- Kume, K., Cantwell, H., Neumann, F. R., Jones, A. W., Snijders, A. P. and Nurse, P.** (2017). A systematic genomic screen implicates nucleocytoplasmic transport and membrane growth in nuclear size control. *PLoS Genet.* **13**, e1006767. doi:10.1371/journal.pgen.1006767
- Kume, K., Cantwell, H., Burrell, A. and Nurse, P.** (2019). Nuclear membrane protein Lem2 regulates nuclear size through membrane flow. *Nat. Commun.* **10**, 1871. doi:10.1038/s41467-019-09623-x
- Laporte, D., Salin, B., Daignan-Fornier, B. and Sagot, I.** (2008). Reversible cytoplasmic localization of the proteasome in quiescent yeast cells. *J. Cell Biol.* **181**, 737-745. doi:10.1083/jcb.200711154
- Laporte, D., Lebaudy, A., Sahin, A., Pinson, B., Ceschin, J., Daignan-Fornier, B. and Sagot, I.** (2011). Metabolic status rather than cell cycle signals control quiescence entry and exit. *J. Cell Biol.* **192**, 949-957. doi:10.1083/jcb.201009028
- Laporte, D., Courtout, F., Salin, B., Ceschin, J. and Sagot, I.** (2013). An array of nuclear microtubules reorganizes the budding yeast nucleus during quiescence. *J. Cell Biol.* **203**, 585-594. doi:10.1083/jcb.201306075
- Laporte, D., Courtout, F., Pinson, B., Dompierre, J., Salin, B., Brocard, L. and Sagot, I.** (2015). A stable microtubule array drives fission yeast polarity reestablishment upon quiescence exit. *J. Cell Biol.* **210**, 99-113. doi:10.1083/jcb.201502025
- Laporte, D., Courtout, F., Tollis, S. and Sagot, I.** (2016). Quiescent *Saccharomyces cerevisiae* forms telomere hyperclusters at the nuclear membrane vicinity through a multifaceted mechanism involving Esc1, the Sir complex, and chromatin condensation. *Mol. Biol. Cell* **27**, 1875-1884. doi:10.1091/mbc.e16-01-0069
- Lemière, J., Real-Calderon, P., Holt, L. J., Fai, T. G. and Chang, F.** (2022). Control of nuclear size by osmotic forces in *Schizosaccharomyces pombe*. *eLife* **11**, e76075. doi:10.7554/eLife.76075
- Liu, J., Hebert, M. D., Ye, Y., Templeton, D. J., Kung, H. and Matera, A. G.** (2000). Cell cycle-dependent localization of the CDK2-cyclin E complex in Cajal (coiled) bodies. *J. Cell Sci.* **113**, 1543-1552. doi:10.1242/jcs.113.9.1543
- Marescal, O. and Cheeseman, I. M.** (2020). Cellular mechanisms and regulation of quiescence. *Dev. Cell* **55**, 259-271. doi:10.1016/j.devcel.2020.09.029
- Marguerat, S., Schmidt, A., Codlin, S., Chen, W., Aebersold, R. and Bähler, J.** (2012). Quantitative analysis of fission yeast transcriptomes and proteomes in proliferating and quiescent cells. *Cell* **151**, 671-683. doi:10.1016/j.cell.2012.09.019
- Masuda, F., Ishii, M., Mori, A., Uehara, L., Yanagida, M., Takeda, K. and Saitoh, S.** (2016). Glucose restriction induces transient G2 cell cycle arrest extending cellular chronological lifespan. *Sci. Rep.* **6**, 19629. doi:10.1038/srep19629
- Matson, J. P. and Cook, J. G.** (2017). Cell cycle proliferation decisions: the impact of single cell analyses. *FEBS J.* **284**, 362-375. doi:10.1111/febs.13898
- Matsuhara, H. and Yamamoto, A.** (2016). Autophagy is required for efficient meiosis progression and proper meiotic chromosome segregation in fission yeast. *Genes Cells* **21**, 65-87. doi:10.1111/gtc.12320
- Moreno, S., Hayles, J. and Nurse, P.** (1989). Regulation of p34 cdc2 protein kinase during mitosis. *Cell* **58**, 361-372. doi:10.1016/0092-8674(89)90850-7
- Moreno, S., Klar, A. and Nurse, P.** (1991). Molecular genetic analysis of fission yeast *Schizosaccharomyces pombe*. *Methods Enzymol.* **194**, 795-823. doi:10.1016/0076-6879(91)94059-L
- Moreno-Torres, M., Jaquenoud, M. and De Virgilio, C.** (2015). TORC1 controls G1-S cell cycle transition in yeast via Mpk1 and the greatwall kinase pathway. *Nat. Commun.* **6**, 8256. doi:10.1038/ncomms9256

- Nabeshima, K., Nakagawa, T., Straight, A. F., Murray, A., Chikashige, Y., Yamashita, Y. M., Hiraoka, Y. and Yanagida, M. (1998). Dynamics of centromeres during metaphase–anaphase transition in fission yeast: Dis1 is implicated in force balance in metaphase bipolar spindle. *Mol. Biol. Cell* **9**, 3211–3225. doi:10.1091/mbc.9.11.3211
- Nambu, M., Kishikawa, A., Yamada, T., Ichikawa, K., Kira, Y., Itabashi, Y., Honda, A., Yamada, K., Murakami, H. and Yamamoto, A. (2022). Direct evaluation of cohesin-mediated sister kinetochore associations at meiosis I in fission yeast. *J. Cell Sci.* **135**, jcs259102. doi:10.1242/jcs.259102
- Narayanaswamy, R., Levy, M., Tsechansky, M., Stovall, G. M., O'Connell, J. D., Mirrielees, J., Ellington, A. D. and Marcotte, E. M. (2009). Widespread reorganization of metabolic enzymes into reversible assemblies upon nutrient starvation. *Proc. Natl. Acad. Sci. USA* **106**, 10147–10152. doi:10.1073/pnas.0812771106
- Neumann, F. R. and Nurse, P. (2007). Nuclear size control in fission yeast. *J. Cell Biol.* **179**, 593–600. doi:10.1083/jcb.200708054
- Nostramo, R., Varia, S. N., Zhang, B., Emerson, M. M. and Herman, P. K. (2016). The catalytic activity of the Ubp3 deubiquitinating protease is required for efficient stress granule assembly in *Saccharomyces cerevisiae*. *Mol. Cell Biol.* **36**, 173–183. doi:10.1128/MCB.00609-15
- O'Farrell, P. H. (2011). Quiescence: early evolutionary origins and universality do not imply uniformity. *Philos. Trans. R. Soc. B Biol. Sci.* **366**, 3498–3507. doi:10.1098/rstb.2011.0079
- Pajalunga, D., Mazzola, A., Salzano, A. M., Biferi, M. G., De Luca, G. and Crescenzi, M. (2007). Critical requirement for cell cycle inhibitors in sustaining nonproliferative states. *J. Cell Biol.* **176**, 807–818. doi:10.1083/jcb.200608109
- Petersen, J. and Nurse, P. (2007). TOR signalling regulates mitotic commitment through the stress MAP kinase pathway and the Polo and Cdc2 kinases. *Nat. Cell Biol.* **9**, 1263–1272. doi:10.1038/ncb1646
- Pino, M. R., Nuñez, I., Chen, C., Das, M. E., Wiley, D. J., D'Urso, G., Buchwald, P., Vavylonis, D. and Verdea, F. (2021). Cdc42 GTPase-activating proteins (GAPs) regulate generational inheritance of cell polarity and cell shape in fission yeast. *Mol. Biol. Cell* **32**, ar14. doi:10.1091/mbc.E20-10-0666
- Piñón, R. (1978). Folded chromosomes in non-cycling yeast cells: evidence for a characteristic g0 form. *Chromosoma* **67**, 263–274. doi:10.1007/BF02569039
- Pluskal, T., Hayashi, T., Saitoh, S., Fujisawa, A. and Yanagida, M. (2011). Specific biomarkers for stochastic division patterns and starvation-induced quiescence under limited glucose levels in fission yeast. *FEBS J.* **278**, 1299–1315. doi:10.1111/j.1742-4658.2011.08050.x
- Rawlings, J. S., Gatzka, M., Thomas, P. G. and Ihle, J. N. (2011). Chromatin condensation via the condensin II complex is required for peripheral T-cell quiescence. *EMBO J.* **30**, 263–276. doi:10.1038/emboj.2010.314
- Reynolds, R. C., Montgomer, P. O. and Hughes, B. (1964). Nucleolar 'caps' produced by actinomycin D. *Cancer Res.* **24**, 1269–1277.
- Rittershaus, E. S. C., Baek, S.-H. and Sasseti, C. M. (2013). The normalcy of dormancy: common themes in microbial quiescence. *Cell Host Microbe* **13**, 643–651. doi:10.1016/j.chom.2013.05.012
- Roche, B., Arcangioli, B. and Martienssen, R. A. (2016). RNA interference is essential for cellular quiescence. *Science* **354**, aah5651. doi:10.1126/science.aah5651
- Roche, B., Arcangioli, B. and Martienssen, R. (2017). Transcriptional reprogramming in cellular quiescence. *RNA Biol.* **14**, 843–853. doi:10.1080/15476286.2017.1327510
- Rutledge, M. T., Russo, M., Belton, J.-M., Dekker, J. and Broach, J. R. (2015). The yeast genome undergoes significant topological reorganization in quiescence. *Nucleic Acids Res.* **43**, 8299–8313. doi:10.1093/nar/gkv723
- Sagot, I. and Laporte, D. (2019). The cell biology of quiescent yeast - a diversity of individual scenarios. *J. Cell Sci.* **132**, jcs213025. doi:10.1242/jcs.213025
- Sagot, I., Pinson, B., Salin, B. and Daignan-Fornier, B. (2006). Actin bodies in yeast quiescent cells: an immediately available actin reserve? *Mol. Biol. Cell* **17**, 4645–4655. doi:10.1091/mbc.e06-04-0282
- Sajiki, K., Hatanaka, M., Nakamura, T., Takeda, K., Shimanuki, M., Yoshida, T., Hanyu, Y., Hayashi, T., Nakaseko, Y. and Yanagida, M. (2009). Genetic control of cellular quiescence in *S. pombe*. *J. Cell Sci.* **122**, 1418–1429. doi:10.1242/jcs.046466
- Schäfer, G., Mcevoy, C. R. E. and Patterson, H.-G. (2008). The *Saccharomyces cerevisiae* linker histone Hho1p is essential for chromatin compaction in stationary phase and is displaced by transcription. *Proc. Natl. Acad. Sci. USA* **105**, 14838–14843. doi:10.1073/pnas.0806337105
- Scheer, U. and Rose, K. M. (1984). Localization of RNA polymerase I in interphase cells and mitotic chromosomes by light and electron microscopic immunocytochemistry. *Proc. Natl. Acad. Sci. USA* **81**, 1431–1435. doi:10.1073/pnas.81.5.1431
- Schneider, C. A., Rasband, W. S. and Eliceiri, K. W. (2012). NIH Image to ImageJ: 25 years of image analysis. *Nat. Methods* **9**, 671–675. doi:10.1038/nmeth.2089
- Shah, K. H., Nostramo, R., Zhang, B., Varia, S. N., Klett, B. M. and Herman, P. K. (2014). Protein kinases are associated with multiple, distinct cytoplasmic granules in quiescent yeast cells. *Genetics* **198**, 1495–1512. doi:10.1534/genetics.114.172031
- Shav-Tal, Y., Blechman, J., Darzacq, X., Montagna, C., Dye, B. T., Patton, J. G., Singer, R. H. and Zipori, D. (2005). Dynamic sorting of nuclear components into distinct nucleolar caps during transcriptional inhibition. *Mol. Biol. Cell* **16**, 2395–2413. doi:10.1091/mbc.e04-11-0992
- Simanis, V. and Nurse, P. (1986). The cell cycle control gene *cdc2⁺* of fission yeast encodes a protein kinase potentially regulated by phosphorylation. *Cell* **45**, 261–268. doi:10.1016/0092-8674(86)90390-9
- Sirri, V., Hernandez-Verdun, D. and Roussel, P. (2002). Cyclin-dependent kinases govern formation and maintenance of the nucleolus. *J. Cell Biol.* **156**, 969–981. doi:10.1083/jcb.200201024
- Spencer, S. L., Cappell, S. D., Tsai, F.-C., Overton, K. W., Wang, C. L. and Meyer, T. (2013). The proliferation-quiescence decision is controlled by a bifurcation in CDK2 activity at mitotic exit. *Cell* **155**, 369–383. doi:10.1016/j.cell.2013.08.062
- Strobl, G. (2007). *The Physics of Polymers: Concepts for Understanding their Structures and Behavior*. Berlin, Germany: Springer Berlin Heidelberg.
- Su, S. S., Tanaka, Y., Samejima, I., Tanaka, K. and Yanagida, M. (1996). A nitrogen starvation-induced dormant G0 state in fission yeast: the establishment from uncommitted G1 state and its delay for return to proliferation. *J. Cell Sci.* **109**, 1347–1357. doi:10.1242/jcs.109.6.1347
- Sun, D. and Buttitta, L. (2017). States of G0 and the proliferation-quiescence decision in cells, tissues and during development. *Int. J. Dev. Biol.* **61**, 357–366. doi:10.1387/ijdb.160343LB
- Sun, S. and Gresham, D. (2021). Cellular quiescence in budding yeast. *Yeast* **38**, 12–29. doi:10.1002/yea.3545
- Sun, X., Hirai, G., Ueki, M., Hirota, H., Wang, Q., Hongo, Y., Nakamura, T., Hitora, Y., Takahashi, H., Sodeoka, M. et al. (2016). Identification of novel secreted fatty acids that regulate nitrogen catabolite repression in fission yeast. *Sci. Rep.* **6**, 20856. doi:10.1038/srep20856
- Swygert, S. G., Kim, S., Wu, X., Fu, T., Hsieh, T.-H., Rando, O. J., Eisenman, R. N., Shendure, J., Mcknight, J. N. and Tsukiyama, T. (2019). Condensin-dependent chromatin compaction represses transcription globally during quiescence. *Mol. Cell* **73**, 533–546.e4. doi:10.1016/j.molcel.2018.11.020
- Tatebe, H. and Yanagida, M. (2000). Cut8, essential for anaphase, controls localization of 26S proteasome, facilitating destruction of cyclin and Cut2. *Curr. Biol.* **10**, 1329–1338. doi:10.1016/S0960-9822(00)00773-9
- Tesio, M. and Trumpp, A. (2011). Breaking the cell cycle of HSCs by p57 and friends. *Cell Stem Cell* **9**, 187–192. doi:10.1016/j.stem.2011.08.005
- Thadani, R., Uhlmann, F. and Heeger, S. (2012). Condensin, chromatin crossbaring and chromosome condensation. *Curr. Biol.* **22**, R1012–R1021. doi:10.1016/j.cub.2012.10.023
- Toda, T., Yamamoto, M. and Yanagida, M. (1981). Sequential alterations in the nuclear chromatin region during mitosis of the fission yeast *Schizosaccharomyces pombe*: video fluorescence microscopy of synchronously growing wild-type and cold-sensitive *cdc* mutants by using a DNA-binding fluorescent probe. *J. Cell Sci.* **52**, 271–287. doi:10.1242/jcs.52.1.271
- Turner, J. J., Ewald, J. C. and Skotheim, J. M. (2012). Cell size control in yeast. *Curr. Biol.* **22**, R350–R359. doi:10.1016/j.cub.2012.02.041
- Valcourt, J. R., Lemons, J. M. S., Haley, E. M., Kojima, M., Demuren, O. O. and Collier, H. A. (2012). Staying alive. *Cell Cycle* **11**, 1680–1696. doi:10.4161/cc.19879
- Van Velthoven, C. T. J. and Rando, T. A. (2019). Stem cell quiescence: dynamism, restraint, and cellular idling. *Cell Stem Cell* **24**, 213–225. doi:10.1016/j.stem.2019.01.001
- Velappan, Y., Signorelli, S. and Considine, M. J. (2017). Cell cycle arrest in plants: what distinguishes quiescence, dormancy and differentiated G1? *Ann. Bot.* **120**, 495–509. doi:10.1093/aob/mcx082
- Wakiya, M., Nishi, E., Kawai, S., Yamada, K., Katsumata, K., Hirayasu, A., Itabashi, Y. and Yamamoto, A. (2021). Chiasmata and the kinetochore component Dam1 are crucial for elimination of erroneous chromosome attachments and centromere oscillation at meiosis I. *Open Biol.* **11**, 200308. doi:10.1098/rsob.200308
- Werner-Washburne, M., Braun, E., Johnston, G. C. and Singer, R. A. (1993). Stationary phase in the yeast *Saccharomyces cerevisiae*. *Microbiol. Rev.* **57**, 383–401. doi:10.1128/mr.57.2.383-401.1993
- Yamamoto, A. and Hiraoka, Y. (2003). Monopolar spindle attachment of sister chromatids is ensured by two distinct mechanisms at the first meiotic division in fission yeast. *EMBO J.* **22**, 2284–2296. doi:10.1093/emboj/cdg222
- Yanagida, M. (2009). Cellular quiescence: are controlling genes conserved? *Trends Cell Biol.* **19**, 705–715. doi:10.1016/j.tcb.2009.09.006
- Yanagida, M., Ikai, N., Shimanuki, M. and Sajiki, K. (2011). Nutrient limitations alter cell division control and chromosome segregation through growth-related kinases and phosphatases. *Philos. Trans. R. Soc. B Biol. Sci.* **366**, 3508–3520. doi:10.1098/rstb.2011.0124
- Yoshida, M., Katsuyama, S., Tateho, K., Nakamura, H., Miyoshi, J., Ohba, T., Matsuhara, H., Miki, F., Okazaki, K., Haraguchi, T. et al. (2013). Microtubule-organizing center formation at telomeres induces meiotic telomere clustering. *J. Cell Biol.* **200**, 385–395. doi:10.1083/jcb.201207168

Zhao, Z., Dammert, M. A., Hoppe, S., Bierhoff, H. and Grummt, I. (2016). Heat shock represses rRNA synthesis by inactivation of TIF-IA and lncRNA-dependent changes in nucleosome positioning. *Nucleic Acids Res.* **44**, 8144-8152. doi:10.1093/nar/gkw496

Zinzalla, V., Graziola, M., Mastriani, A., Vanoni, M. and Alberghina, L. (2007). Rapamycin-mediated G1 arrest involves regulation of the Cdk inhibitor Sic1 in

Saccharomyces cerevisiae. *Mol. Microbiol.* **63**, 1482-1494. doi:10.1111/j.1365-2958.2007.05599.x

Zuin, A., Carmona, M., Morales-Ivorra, I., Gabrielli, N., Vivancos, A. P., Ayté, J. and Hidalgo, E. (2010). Lifespan extension by calorie restriction relies on the Sty1 MAP kinase stress pathway. *EMBO J.* **29**, 981-991. doi:10.1038/emboj.2009.407